

# Multi-scale Vehicle Localization In Heterogeneous Mobile Communication Networks

Lele Cong, Kaitao Meng, *Member, IEEE*, Deshi Li, Hao Jiang, *Member, IEEE*, and Liang Xu

**Abstract**—Low-latency and high-precision vehicle localization plays a significant role in enhancing traffic safety and improving traffic management for intelligent transportation. However, in complex road environments, the low latency and high precision requirements could not always be fulfilled due to the high complexity of localization computation. To tackle this issue, we propose a road-aware localization mechanism in heterogeneous networks (HetNet) of the mobile communication system, which enables real-time acquisition of vehicular position information, including the vehicular current road, segment within the road, and coordinates. By employing this multi-scale localization approach, the computational complexity can be greatly reduced while ensuring accurate positioning. Specifically, to reduce positioning search complexity and ensure positioning precision, roads are partitioned into low-dimensional segments with unequal lengths by the proposed singular point (SP) segmentation method. To reduce feature-matching complexity, distinctive salient features (SFs) are extracted sparsely representing roads and segments, which can eliminate redundant features while maximizing the feature information gain. The Cramér-Rao Lower Bound (CRLB) of vehicle positioning errors is derived to verify the positioning accuracy improvement brought from the segment partition and SF extraction. Additionally, through SF matching by integrating the inclusion and adjacency position relationships, a multi-scale vehicle localization (MSVL) algorithm is proposed to identify vehicular road signal patterns and determine the real-time segment and coordinates. Simulation results show that the proposed multi-scale localization mechanism can achieve lower latency and high precision compared to the benchmark schemes.

**Index Terms**—vehicle localization, low latency, multiple scales, salient feature (SF), heterogeneous networks (HetNet)

## I. INTRODUCTION

Vehicle localization plays a vital role to enhance road safety, optimize path planning, and improve traffic management for intelligent transportation [1]. There is a high demand for vehicle localization services on roads, where vehicle localization accounted for more than 90% of road-related localization services [2]. Especially, to ensure road traffic safety, low-latency and high-precision localization is essential for high-speed vehicles. However, low-latency vehicular localization could not always be fulfilled without sacrificing positioning

precision due to complex positioning computation. With the integration of the global positioning system (GPS) inside vehicles, satellite navigation technology has been widely used for vehicle localization. However, the responding time and positioning precision of GPS are affected by satellite transmission path loss, especially in severe weather and dense obstructions scenarios [3]. Although the inertial navigation system (INS) can locate vehicles through dead reckoning, the long-term state prediction would inevitably lead to cumulative errors, which may decrease localization precision [4]. Considering that the position of the in-vehicle communication equipment and the vehicular user equipment (VUE) remains relatively stationary with the vehicular position, the vehicular position can be equivalently estimated by locating the VUE. With seamless coverage and accessibility, cellular networks can provide alternative opportunities for VUE localization to reduce latency and guarantee localization precision [5].

Based on cellular network signals, three typical positioning methods can be used for VUE localization, i.e., Cell ID-based methods [6–10], geometric-based methods [11–22], and fingerprint-based methods [23–30]. Though the delay of Cell ID-based methods can be shortened by obtaining a serving cell position, the accuracy relies on the serving cell radius [6]. To enhance the localization precision, radio frequency (RF) signal information, such as received signal strength (RSS), time of arrival (TOA), time difference of arrival (TDOA), or angle of arrival (AOA) can be utilized for VUE positioning through geometric-based methods [11]. Nevertheless, since the explicit line-of-sight (LoS) links between base stations (BSs) and VUE are difficult to maintain in complex road environments, e.g., tunnels and overpasses, the localization accuracy of geometric-based methods may be severely degraded [12]. Moreover, multiple distance estimation computations between VUE and BSs result in intolerable response delays [13]. Without relying on complex signal information and LoS links, fine-grained RF signals from multiple transmitters, e.g., Wi-Fi access points (APs) and BSs can be extracted to locate VUE through fingerprint matching [23], [24]. However, fine-grained fingerprint matching is extremely time-consuming to ensure vehicular localization precision in wide outdoor environments [25], [26]. Additionally, the faint decay of millimeter waves according to various environments would greatly affect localization performance [31]. With rapidly growing demands for high-reliability and low-latency mobile communication services, the heterogeneous networks (HetNet) BSs including the fourth generation (4G) and the fifth generation (5G) BSs have been widely deployed to improve network performance [32]. Recent research in mobile networks tended to strengthen localization

The work of Kaitao Meng was supported in part by UKRI under Grant EP/Y02785X/1. This work was supported in part by the National Key R&D Program of China under Grant 2023YFE0206600 and Grant 2022YFB2901202 and in part by the Fundamental Research Funds for the Central Universities under Grant 2042024kf1006. (Corresponding author: Kaitao Meng; Hao Jiang.)

Lele Cong, Deshi Li, Hao Jiang, and Liang Xu are with the School of Electronic Information, Wuhan University, Wuhan 430072, China. (emails: conglele@whu.edu.cn; dsli@whu.edu.cn; jh@whu.edu.cn; lgxu@whu.edu.cn).

Kaitao Meng is with the Department of Electronic and Electrical Engineering, University College London, UK (email: kaitao.meng@ucl.ac.uk).

precision by intelligent reflective surfaces [33] and ultra-massive MIMO [34], etc., while overlooking the potential of HetNet to reduce localization latency [35]. Moreover, there are different fluctuation patterns of HetNet signals since the signal diffraction capabilities and path loss vary with frequency bands, which presents valuable opportunities for effective vehicle positioning. Therefore, studying vehicle localization in HetNet is urgently needed.

Due to relatively constant positions of signal blockage obstacles along roads, e.g., trees and buildings, signals between BSs and VUE orderly switch between LoS and non-line-of-sight (NLoS) links [36]. Hence, distinctive statistical signal features of HetNet RSS values, e.g., the mean value, the variance value, the signal gradient, etc., can be extracted to represent corresponding road sections. Then, signal feature matching is designed for segment positioning by minimizing the Euclidean distance between the offline extracted signal features and the real-time signal features. However, achieving both low latency and high precision is still challenging due to the following reasons. First, achieving high precision requires fine-grained feature matching, leading to higher computational complexity and longer localization response time. Second, coarse position granularity with sparse signal features could provide low positioning latency, but resulting in high localization errors. Hence, it is critical to reduce feature-matching complexity and ensure localization precision at the same time. Due to the varying spatial distances, carrier frequencies, and signal propagation environments between VUE and HetNet BSs, significant differences in signal gradients can be observed across different road sections, as illustrated in Fig. 1, where a *segment* can be defined as a road section obtained by partitioning the road-scale HetNet signal sequence based on signal gradients. Therefore, high-dimensional coordinates within a road can be grouped into low-dimensional segments with different signal gradients, which can reduce the complexity of position searching within roads and improve road localization precision. As not all statistical signal features significantly differ between roads and segments, to sparsely and accurately represent roads on various scales, *salient features (SFs)* are defined as the statistical features with significant differences among roads and segments, where the significant difference refers to the absolute difference of the normalized features between two adjacent positions exceeding a predetermined threshold. To the best of our knowledge, this is the first time that low-dimensional salient features extraction and multi-scale road representation are realized to locate vehicles in complex urban road environments, which can reduce localization computational complexity and ensure accuracy at the same time. The main contributions in this paper can be summarized as follows:

- We propose a road-aware localization mechanism in HetNet, which includes the HetNet signal feature extraction and multi-scale vehicle localization to enable real-time acquisition of vehicular position information on different spatial scales, i.e., roads, segments, and coordinates.
- We propose a singular point (SP) segmentation method extracting gradient change points for road segmentation,

based on which we then propose a salient feature (SF) extraction method by maximizing feature information gain to extract signal features with significant differences. Moreover, to theoretically verify the improvement of localization accuracy by road partitioning and SF extracting, the Cramér-Rao Lower Bound (CRLB) is derived.

- We propose a multi-scale vehicle localization (MSVL) algorithm, which includes three modules, i.e., the road recognition module, the segment positioning module, and the coordinate localization module. By integrating the spatial inclusion and adjacency properties of roads and segments, the MSVL algorithm can quickly determine the vehicle's multi-scale positions with high precision based on SF matching.
- We conduct real experiments to verify the proposed multi-scale localization mechanism in a real-world HetNet scenario. The experimental results reveal that our proposed mechanism can achieve high positioning precision with low delay.

The remainder of this paper is organized as follows. Section II summarizes the related work and Section III describes the proposed mechanism model and problem formulation. In section IV, HetNet signal sequences are segmented to construct multi-scale positioning space, and SFs are extracted to sparsely represent roads and segments. The multi-scale localization algorithm is designed in section V. Section VI provides numerical results to reveal the performance of our proposed mechanism. Section VII concludes this paper.

*Notations:* A capital bold-face letter denotes a matrix, e.g.,  $\mathbf{W}$ . A vector is denoted by a bold-face lowercase letter, e.g.,  $\mathbf{f}$ . The  $l_2$  norm of a vector is represented by  $\|\cdot\|_2$ . The absolute value of a variable is denoted as  $|\cdot|$ .

## II. RELATE WORK

This section provides an overview of the current literature on cellular network-based localization, specifically focusing on the performance in terms of latency and precision. Three kinds of typical positioning methods based on cellular networks have been investigated, i.e., Cell ID-based methods [7–10], geometric-based methods [14–22], and fingerprint-based methods [27–30].

### A. Cell ID-based Method

Cell ID-based methods localize VUE by obtaining the ID of the VUE's service cell [7]. Though high positioning speed can be achieved due to low computational complexity, the localization precision depends on radius of BS coverage areas. To reduce localization errors, supplementary data such as timing advance (TA) and round-trip time (RTT) are utilized in enhanced Cell-ID methods [8], [9]. Despite this, the enhanced Cell-ID methods remain relatively coarse in precision, typically within tens of meters in urban small-cell networks and several hundred meters in rural macro-cell networks [10].

### B. Geometric-based Method

To improve localization accuracy, geometric-based methods can be used to localize vehicles by distance or angle estimating

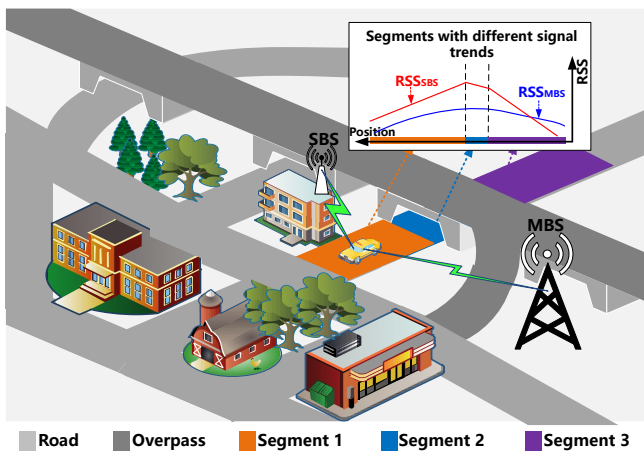


Fig. 1: Road localization scenario in urban area.

between VUE and multiple BSs. Nevertheless, the precision of geometric-based methods is compromised by NLoS links of any BS signals. To reduce the localization errors, the NLoS measurements can be first distinguished by machine learning approaches, e.g., support vector machine (SVM) [14, 15], neural network (NN) [16, 17], and relevance vector machine (RVM) [18]. Then, the localization errors of NLoS links can be mitigated using the least squares method [19], the constrained optimization method [20], the maximum likelihood method [21], and the robust statistics method [22]. However, reducing positioning errors incurs a significant time overhead that increases exponentially as the number of BSs involved grows [13]. Additionally, suppose that LoS links exist between all BSs and the vehicle, intolerable positioning delays may result from multiple distance estimations between the VUE and all BSs.

### C. Fingerprint-based Method

Independent of LoS environments, a fingerprint is defined as a vector of signal strengths from multiple transmitters at grids of known locations, i.e., reference points (RPs) [37]. Then, the basic idea of a fingerprinting approach is to locate a mobile device by comparing its RSSs to a predefined database of fingerprints [38]. Fingerprint-based localization is effective for indoor environments, where GPS signals may be absent or unreliable due to signal blockage or multi-path effects [5]. However, due to fine-grained fingerprint matching, the high computation complexity results in intolerable localization delays. To reduce positioning latency and online computation costs, clustering methods have been proposed to group fingerprints [28], [29]. The author of paper [27] utilized subspace-based techniques to compress the dimension of its fingerprint database. However, on the one hand, a huge amount of human labor would be consumed to collect fingerprints in wide outdoor road environments. On the other hand, a large fingerprint database would consume huge maintenance and update costs if transmitters' numbers, positions, or device types changed [30]. In addition, high fingerprinting localization precision depends on RF signals from as many transmitters as possible, which may not always be fulfilled due to the severe signal attenuation in the 5G and 6G mobile communication systems.

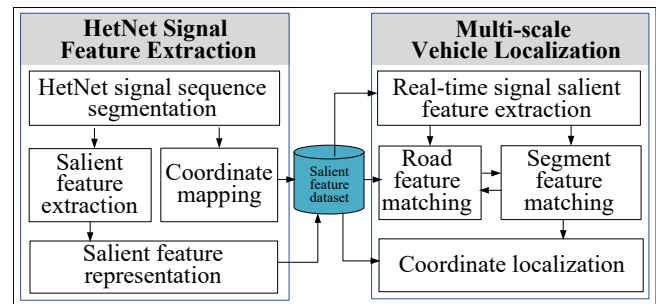


Fig. 2: Road-aware localization mechanism.

The existing positioning methods based on cellular networks mainly focus on reducing positioning errors by complex localization algorithms and ignore positioning delay performance. However, to ensure the traffic safety of high-speed vehicles, both low-latency and high-precision positioning performance are indispensable. Unlike previous positioning methods, we propose a road-aware positioning mechanism by establishing a multi-scale positioning space and extracting salient features to reduce positioning latency while ensuring positioning accuracy.

## III. MECHANISM MODELING AND PROBLEM FORMULATION

### A. Road-aware Localization Mechanism

In complex urban road environments portrayed in Fig. 1, to achieve low-latency localization, we propose a road-aware localization mechanism with the architecture illustrated in Fig. 2. By analyzing the fluctuation trends of HetNet signals under different NLoS and LoS signal propagation conditions, wide road environments can be divided into low-dimensional segments, which construct the multi-scale positioning space including roads and segments. Moreover, due to the change in signal propagation environments and signal propagation distances, distinctive signal features can be extracted for position mapping. The proposed mechanism includes two stages: the HetNet signal feature extraction and the multi-scale vehicle localization.

*HetNet signal feature extraction:* To construct the low-dimension positioning space on multiple scales, roads can be partitioned into segments through HetNet signal sequence segmentation, which would reduce the positioning computation complexity. By extracting SFs from segmented HetNet signal sequences, roads and segments can be sparsely represented to reduce feature-matching complexity. Moreover, the CRLB is derived to verify the positioning accuracy improvement brought by the proposed segment partition and SF extraction.

*Multi-scale vehicle localization:* To accurately locate a vehicular position on roads, the real-time SFs of HetNet signals will be extracted. Then, based on road and segment SF matching, a MSVL algorithm is designed to quickly obtain real-time vehicular positions. To improve vehicle positioning precision, the coordinates within a segment can be localized based on fitted curves.

## B. HetNet Signal Representation

To form road-scale HetNet signal sequences extracting signal features, roads within a SBS coverage area can be defined as a road positioning space  $\mathcal{R}$ , i.e.,  $\mathcal{R} = \{r_1, r_2, \dots, r_m\}$ , where  $r_i$  is a road in  $\mathcal{R}$ , and the number of roads is represented as  $m$ . Within the road positioning space  $\mathcal{R}$ , a road-scale HetNet signal sequence is defined as a vector  $\phi_i$  which is denoted as  $\phi_i = [\mathbf{o}_1, \mathbf{o}_2, \dots, \mathbf{o}_{L_i}]^\top$ , where  $\mathbf{o}_j$  represents a HetNet signal vector of the  $j$ th position on the road  $r_i$ . In  $\phi_i$ ,  $L_i$  denotes the number of signal sampling positions within the road  $r_i$ .  $L_i$  is determined by the signal sampling distance interval  $\Delta D$ . To ensure consistent measurement granularity of signal features for effective road representation and identification,  $\Delta D$  remains constant across different roads and segments. This signal sampling distance interval is influenced by the time interval of the signal sampling and the vehicular velocity. The HetNet signal vector  $\mathbf{o}_j$  takes the form of  $\mathbf{o}_j = [P_{j,1}, P_{j,2}, \dots, P_{j,K}]^\top$ , where  $P_{j,k}$  denotes the RSS of the  $k$ th BS. The number of HetNet BSs is defined as  $K$  including 1 macro BS (MBS) and  $K - 1$  small-cell BSs (SBSs). Based on road-scale HetNet signal sequences and corresponding signal features, our proposed mechanism is designed independent of BS locations and transmit powers locating vehicles, which can save data storage space and computation costs. The coordinate vector of the  $j$ th position is denoted by  $\mathbf{c}_j = (x_j, y_j)^\top$ , where the  $x_j$  and  $y_j$  respectively represent 2 dimensional (2D) coordinates, i.e., longitude and latitude. The RSS of the  $k$ th BS  $P_{j,k}$  (in dBm) on the  $j$ th position is given by [39]:

$$P_{j,k} = P_0 - 10\beta_k \log_{10} \|\mathbf{c}_j - \mathbf{c}_{BS_k}\|_2 + X_k, \quad (1)$$

where  $P_0$  denotes the original RSS at the target, and  $\beta_k$  represents the path loss parameter depending on signal propagation environments.  $X_k$  is the Gaussian white noise. In (1), the position of the  $k$ th BS is denoted by the coordinate vector  $\mathbf{c}_{BS_k} = (x_{BS_k}, y_{BS_k})^\top$ . The signal gradient  $g_{j,k}$  of the  $k$ th HetNet BS can be calculated by the RSS difference value per unit distance, which can be expressed as follows:

$$g_{j,k} = \frac{P_{j+1,k} - P_{j,k}}{\left( (x_{j+1} - x_j)^2 + (y_{j+1} - y_j)^2 \right)^{\frac{1}{2}}}. \quad (2)$$

Within the road  $r_i$ , a segment positioning space  $\mathcal{S}_i$  can be established by partitioning HetNet signal sequence based on signal gradients, i.e.,  $\mathcal{S}_i = \{s_1, s_2, \dots, s_{n_i+1}\}$ , where  $s_l$  represents the  $l$ th segment corresponding to a segment-scale HetNet signal sequence  $\psi_l$ , and  $n_i + 1$  represents the segment number. The  $l$ th segment can be represented by the 2D coordinate vector  $(x_m^l, y_m^l)^\top$ , where  $x_m^l$  and  $y_m^l$  respectively denote the longitude and latitude of the middle position within this segment. Within the segment  $s_l$ , a coordinate space is defined as  $\mathcal{C}_l$  composed by all RSS sampling coordinates, i.e.,  $\mathcal{C}_l = \{\mathbf{c}_1, \mathbf{c}_2, \dots, \mathbf{c}_{N_l}\}$ , where  $N_l$  represents the coordinate number of the segment  $s_l$ . Then, a multi-scale positioning space is established, consisting of roads, segments, and coordinates. In this multi-scale positioning space, the vehicular position vector can be expressed as  $\mathbf{p} = [r_i, s_l, \mathbf{c}_j]^\top$ . Based on corresponding HetNet signal sequences, the road-scale and

segment-scale SF vectors, i.e.,  $\mathbf{f}_{r_i}$  and  $\mathbf{f}_{s_l}$ , can be extracted to represent road  $r_i$  and segment  $s_l$ , respectively. Most notations used in this paper are listed in Table I.

TABLE I:  
IMPORTANT NOTIFICATIONS AND SYMBOLS USED IN THIS WORK

Notation	Physical meaning
$r_i$	Road $i$
$s_l$	Segment $l$
$\mathbf{c}_j$	Coordinate vector at the $j$ th position
$\mathcal{R}$	Road positioning space
$\mathcal{S}_i$	Segment positioning space within the road $r_i$
$\mathcal{C}_l$	Coordinate positioning space within the segment $s_l$
$\phi_i$	HetNet signal sequence of the road $r_i$
$\mathbf{o}_j$	HetNet signal vector at the $j$ th position
$P_{j,k}$	RSS of the $k$ th BS at the $j$ th position
$g_{j,k}$	Signal gradient of the $k$ th BS at the $j$ th position
$x_j$	Longitude at the $j$ th position
$y_j$	Latitude at the $j$ th position
$\beta_k$	Path loss parameter of the $k$ th BS
$\mathbf{c}_{BS_k}$	Coordinate vector of the $k$ th BS position
$X_k$	Gaussian white noise of the $k$ th BS
$\mathbf{f}_{r_i}$	SF vector of the road $r_i$
$\mathbf{f}_{s_l}$	SF vector of the segment $s_l$
$\mathbf{p}$	Multi-scale position vector

## C. Problem Formulation

To achieve low latency and high precision performance, the multi-scale vehicle localization problem can be formulated as follows:

$$\hat{\mathbf{p}} = \arg \max_{r_i, s_l, \mathbf{c}_j} \omega_1 \Pr(r_i) \Pr(\hat{r}_i | r_i) \Pr(s_l | \hat{r}_i) \Pr(\hat{s}_l | s_l) \cdot \Pr(\mathbf{c}_j | \hat{s}_l) + (1 - \omega_1) \left(\frac{O}{V}\right)^{-1} \quad (3)$$

$$\text{s.t. } r_i \in \mathcal{R}, s_l \in \mathcal{S}_i, \mathbf{c}_j \in \mathcal{C}_l, \quad (3a)$$

$$\omega_1 \in [0, 1], \quad (3b)$$

where  $\Pr(r_i) \Pr(\hat{r}_i | r_i) \Pr(s_l | \hat{r}_i) \Pr(\hat{s}_l | s_l) \Pr(\mathbf{c}_j | \hat{s}_l)$  denotes the joint Bayes probability of road matching, segment matching, and coordinate estimation. The ratio  $\frac{O}{V}$  serves as an indicator of computation latency, where  $O$  represents the number of CPU cycles executing the positioning task, which relies on the complexity of the positioning algorithm. Meanwhile,  $V$  denotes the local computing rate of the VUE, quantified as the number of CPU cycles executed per second. In (3),  $\omega_1$  is defined as the weighting factor of localization precision. The weighting factor can be improved for higher positioning accuracy. By optimizing the positioning problem in (3), we aim to minimize the computation latency and maximize the joint Bayes probability of the multi-scale positioning process. Hence, to solve this multi-scale vehicular positioning problem, three key sub-problems need to be solved: how to effectively divide segments with unequal lengths of different roads, how to reduce feature dimension to sparsely and accurately represent multi-scale positions, and how to quickly locate multi-scale positions with high precision.

#### IV. HETNET SIGNAL FEATURE EXTRACTION

In this section, a SP segmentation method and a SF extraction method are proposed to respectively solve the sub-problems of partitioning segments and extracting sparse signal features. Specifically, to construct the segment positioning space, a SP segmentation method is first proposed by partitioning HetNet signal sequences based on signal gradients. Then, a SF extraction method is proposed to represent roads and segments in a sparse way. Meanwhile, the CRLB is derived to verify the positioning accuracy improvement brought from the segment partition and SF extraction. Additionally, to obtain vehicular locations within segments, HetNet signals are mapped to coordinates by curve fitting.

##### A. HetNet Signal Sequence Segmentation

1) *SP Extraction and Sequence Segmentation*: Segment positioning refers to the process of determining the localized segment on which a vehicle is moving. To construct segment positioning space, HetNet signal sequence partition is crucial. Nevertheless, balancing the partitioning lengths and the segment positioning accuracy is challenging. To partition segments with adaptive lengths, gradient features can be applied for partitioning adjacent road sections since signal gradients will change regularly in LoS and NLoS links in different road sections caused by fixed regional obstacles [40], e.g., trees, buildings, bridges, etc. To accurately partition each road based on signal gradient features, the SP is defined, and then a segmentation method is designed by extracting SPs of HetNet signal sequences.

For ease of analysis, we give the definitions of SPs as follows:

**Definition 1 (SP)**: SPs are defined as HetNet signal vectors employed to partition the roads into segments as (4), where the signal gradient symbol or value of at least one BS changes at each SP as qualified in (5).

$$\phi_i = \underbrace{[\mathbf{o}_1, \mathbf{o}_2, \dots, \mathbf{o}_{L_i}]^\top}_{\text{Road } r_i} = \underbrace{[[\mathbf{o}_1, \dots, \mathbf{o}_{b_1}]]}_{\text{Segment } s_1}^{\text{SP}_1}, \quad (4)$$

$$\underbrace{[\mathbf{o}_{b_1+1}, \dots, \mathbf{o}_{b_2}]}_{\text{Segment } s_2}^{\text{SP}_2}, \dots, \underbrace{[\mathbf{o}_{b_{n_i}}, \dots, \mathbf{o}_{L_i}]}_{\text{Segment } s_{n_i+1}}^{\text{SP}_{n_i}}$$

where  $\phi_i$  is the HetNet signal sequence collected from the road  $r_i$ . A segment is represented by a HetNet signal sequence, where the endpoints of this sequence are SPs. In (4),  $b_j$  ( $b_j \in [1, L_i]$ ) is the position index of the SP, where  $L_i$  is the position number within the road  $r_i$ . At the  $b_j$ th signal sampling position, the SP is denoted by the vector of HetNet RSSs, i.e.,  $\mathbf{o}_{b_j} = [P_{b_j,1}, P_{b_j,2}, \dots, P_{b_j,K}]^\top$ . In (4),  $n_i$  denotes the number of SPs that varies with roads. Since SPs essentially represent key change points of the signs or the values in gradient features, the length of a SP set  $n_i$  is determined by the number of extreme points of a HetNet signal sequence and the change threshold of gradient values. To ensure that there exist  $n_i$  SPs to partition a road into multiple segments as (4),  $n_i$  fulfills the condition  $n_i \in [0, L_i - 2]$ , where  $n_i = 0$  denotes that there is no gradient change of any BS signals

within the road, and  $n_i = L_i - 2$  indicates that the signal gradient difference on both sides of each signal sampling position on the road is greater than the threshold. To accurately describe the sign or the value change of the gradient feature, for  $\forall b_j \in [1, L_i], \forall k \in [1, K]$ , the signal gradient at each SP is constrained as follows:

$$\begin{cases} \text{sgn}(g_{b_j+1,k} \cdot g_{b_j,k}) < 0, \\ \text{or}, \\ |g_{b_j+1,k} - g_{b_j,k}| \geq \tau, \end{cases} \quad (5)$$

where  $g_{b_j+1,k}$  and  $g_{b_j,k}$  respectively denote the signal gradients of the  $k$ th BS on two adjacent positions, and  $\tau$  represents the gradient change threshold. In (5),  $\text{sgn}(g_{b_j+1,k} \cdot g_{b_j,k}) < 0$  and  $|g_{b_j+1,k} - g_{b_j,k}| \geq \tau$  respectively determine the sign and value changes of the gradient at a SP. By the gradient constraint in (5), the gradient sign or the gradient value of at least one BS signal changes. Based on the SP definition in (4) and (5), the position index set of all SPs within a road-scale HetNet signal sequence  $\phi_i$  is denoted as  $\mathcal{B}_i = \{b_1, b_2, \dots, b_{n_i}\}$ . This position index set  $\mathcal{B}_i$  can be used to extract all SPs within a road.

Due to the varying lengths and shapes of roads, the number of SPs also differs, resulting in segments with different lengths. To accurately partition different roads, we propose a SP segmentation method. This method first extracts the position index set  $\mathcal{B}_i$ , and then partition this road based on the SPs of  $\mathcal{B}_i$ . Specifically, to improve the anti-noise performance and avoid the cancellation of signals at adjacent positions during the calculation of the average gradient, the signed mean square gradient feature is employed to partition roads. Based on the signed mean square gradient features, the sequence segmentation method can be designed by extracting the position index set of SPs as follows:

$$\mathcal{B}^* = \arg \min_{\mathcal{B}} \sum_{k=1}^K \sum_{j=b_l}^{b_{l+1}} \frac{(\text{sgn}(P_{j+1,k} - P_{j,k})g_{j,k}^2 - \overline{g_{b_l, b_{l+1}, k}^2})^2}{b_{l+1} - b_l + 1}, \quad (6)$$

where  $K$  is the number of all HetNet BSs, and  $g_{j,k}$  denotes the signal gradient feature as (2).  $\text{sgn}(P_{j+1,k} - P_{j,k})$  represents the sign function which is utilized to determine the sign of the gradient at adjacent positions as follows:

$$\text{sgn}(P_{j+1,k} - P_{j,k}) = \begin{cases} 1 & P_{j+1,k} - P_{j,k} > 0 \\ 0 & P_{j+1,k} - P_{j,k} = 0 \\ -1 & P_{j+1,k} - P_{j,k} < 0 \end{cases} \quad (7)$$

$\overline{g_{b_l, b_{l+1}, k}^2}$  denotes the average value of the signed mean square gradient of the  $k$ th BS between the  $b_l$ th position and  $(b_l + 1)$ th position, which can be expressed as follows:

$$\overline{g_{b_l, b_{l+1}, k}^2} = \frac{1}{b_{l+1} - b_l + 1} \sum_{j=b_l}^{b_{l+1}} \text{sgn}(P_{j+1,k} - P_{j,k})g_{j,k}^2. \quad (8)$$

Extracting  $\mathcal{B}^*$  is highly non-trivial since SPs determine the length of the partitioned segments and the accuracy of the segment features. To extract the optimal position index set  $\mathcal{B}^*$  within the HetNet signal sequence  $\phi_i$ , the Bottom-up algorithm [41] is utilized.

To demonstrate that our proposed method can effectively

extract SPs that satisfy their definitions in (4) and (5), the SP partitioned segment-scale HetNet signal sequences and corresponding gradient signal features are shown in Fig. 3. If all  $b_l$  and  $b_{l+1}$  are extracted according to Fig. 3(b), the optimal solution for segment 1's SPs position indexes is 1 and 48. However, if 1 and 60 are chosen as the SFs of segment 1, the gradient variance in (6) will increase, making it challenging to achieve the goal of minimizing the sum of gradient variance. Therefore, the extracted SPs of (6) can meet the gradient constraint of SP definition in (5), and road-scale HetNet signal sequence can be automatically partitioned into segments with different gradients.

Based on two adjacent position indexes of the extracted SPs, a road-scale HetNet signal sequence  $\phi_i$  can be partitioned into multiple segment-scale HetNet RSS sequences, i.e.,  $\hat{\phi}_i = \{\psi_1, \dots, \psi_{n_i+1}\}$ , where  $\psi_l = \{\mathcal{O}_{b_l}, \dots, \mathcal{O}_{b_{l+1}}\}$ , and  $n_i + 1$  denotes the number of partitioned segment-scale HetNet RSS sequences. Corresponding to segment-scale HetNet signal sequences in  $\hat{\phi}_i$ , segments within road  $r_i$  can be partitioned, and these segments are defined as a segment space  $\mathcal{S}_i = \{s_1, s_2, \dots, s_{n_i+1}\}$ , where  $s_l$  denotes the  $l$ th segment on the road  $r_i$ .

2) *Segmentation Bound Derivation and Proof*: To analyze positioning errors of different segmentation bounds, the CRLB of segment positioning is derived. Based on the signed mean square gradient  $g_j^l$  of the  $l$ th segment, the CRLB takes the form

$$tr(\text{CRLB}) \geq \frac{\ln^2 10}{\frac{4 \cdot 10^4}{(N_l - 1)^2} \sum_{k=1}^K \frac{\beta_k^{l,4}}{\rho_k^{l,2}} \left( \frac{1}{d_{N_l,k}^l} - \frac{1}{d_{1,k}^l} \frac{1}{N_l} \right)^2}, \quad (9)$$

where  $\beta_k^l$  and  $\rho_k^{l,2}$  respectively represent the path-loss exponent and the RSS noise covariance of the  $k$ th BS within the  $l$ th segment. The endpoints of a segment are defined as the beginning and the end HetNet RSS vectors of this segment-scale HetNet signal sequence. In (9),  $d_{N_l,k}^l$  and  $d_{1,k}^l$  represent signal propagation distances of the  $l$ th segment endpoints, which are decided by the extracted SPs of the proposed sequence segmentation method.  $N_l$  denotes the number of signal sampling positions within the  $l$ th segment. The detailed CRLB calculation of (9) is presented in Appendix A.

If the signal propagation environments within a segment remain stable, the derivation of the CRLB in (9) demonstrates that the minimum achievable positioning error is intrinsically linked to the signal propagation distances at the points where the segment is partitioned. Based on the path-loss model in (1), the RSS values can be utilized to calculate corresponding signal propagation distances. To achieve the lowest CRLB,  $P_{N_l,k}^l$  and  $P_{1,k}^l$  respectively represent the RSS values of the  $k$ th BS at the endpoints of the  $l$ th segment RSS sequence. Meanwhile,  $P_{max,k}^l$  and  $P_{min,k}^l$  represent the extreme points, which are the maximum and minimum RSSs of the  $k$ th BS signals within the  $l$ th segment RSS sequence. The difference between endpoints and extreme points of segment RSS sequence is that endpoints represent the beginning and the end points which can be any RSS values, but the extreme points only denote the maximum and minimum RSS values within the HetNet signal sequence. The CRLB of the segment partitioned by the RSS extreme

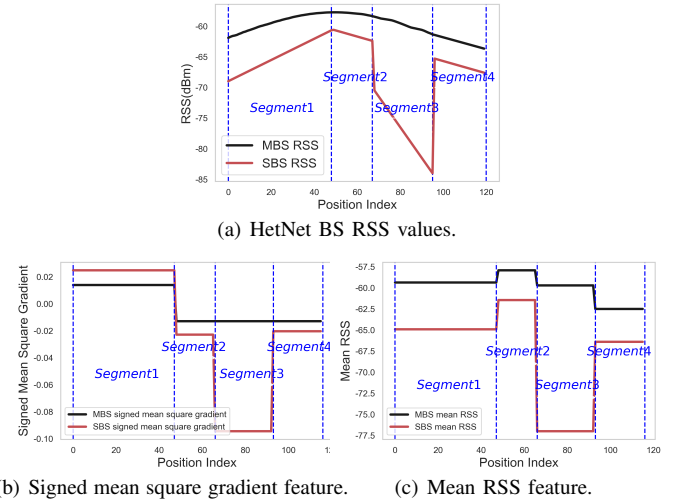


Fig. 3: An example of HetNet signals along a road.

points is expressed as  $\text{CRLB}_{P'}$ , and  $\text{CRLB}_P$  represents the CRLB of the segment that is not divided by the RSS extreme points. Therefore, Proposition 1 is proposed to prove that the segments approaching the lowest CRLB can be obtained by the SPs that are the extreme points of a road-scale HetNet signal sequence.

**Proposition 1:** With the same path-loss exponent  $\beta_k^l$ , if the beginning point and the end point of one segment-scale signal sequence from the  $k$ th BS respectively satisfies  $P_{N_l,k}^{l'} = P_{max,k}^l$  and  $P_{1,k}^{l'} = P_{min,k}^l$ ,  $\text{CRLB}_{P'} < \text{CRLB}_P$ .

*Proof:* Please refer to Appendix B. ■

As derived in Proposition 1, when the endpoints of a segment HetNet signal sequence are the extreme points of the road-scale HetNet RSS sequence, the segment can be accurately located approaching the lowest positioning error.

Since the path-loss exponent  $\beta_k^l$  can influence RSS measurements, it is important to investigate the gradient turning points, which are the other type of SPs, to ensure an accurate segment partition. To this end, we propose the Remark 1 to analyze the impact of signal propagation environments on segment partitioning.

**Remark 1:** To approach the lowest CRLB, a segment signal sequence can be further partitioned based on the gradient turning points of the  $k$ th BS signals if the  $\beta_k^l$  changed within a segment.

Based on the Remark 1, the signal path-loss exponent  $\beta_k^l$  is stable within the segmented signal sequences. In this case, road-scale signal sequences can be partitioned into segment signal sequences approaching the lowest CRLB as (9).

### B. Signal Feature Extraction and Representation

Due to the high-dimensional signals in the segmented HetNet signal sequences, a feature set composed of signal statistical features can be extracted to represent roads and segments. However, not all features have obvious distinctions between different road-scale signal sequences. If the signal features with significant differences could be extracted for feature matching, not only would the matching accuracy be improved, but also would the computation complexity be reduced. To this end, the road and segment representation



consists of three processes, namely feature set extraction, SF extraction, and sparse feature representation.

1) **Feature Set Extraction:** Representing long roads by a single gradient feature is challenging since complex signal fluctuation trends exist along roads caused by different signal attenuation strengths of HetNet signals. Hence, it is critical to represent roads with multiple signal features to improve the representation accuracy. Then, using what kind of features is beneficial for our proposed mechanism? Since RSS values of HetNet signals can be obtained without additional information on BS locations and transmission powers, statistical signal features are extracted from HetNet RSSs, which can save the storage space and alleviate the computational burden on resource-limited mobile devices. Moreover, as the received signal power is essentially obtained by the average amplitude of different frequency sub-carriers, the RSS level can reflect the amplitude feature of the signal's frequency domain and indicate path loss related to the environment and distance. Therefore, by extracting RSS features from multiple BSs, the adverse effects on positioning accuracy can be mitigated though there are frequency domain feature fluctuations of a single BS. To accurately reflect the signal features of different roads, various statistical features of HetNet RSSs can be extracted to form a feature set.

To characterize high-dimensional signal data of roads by only a few signal features, a feature set is extracted including the statistical signal features and correlation signal features. To avoid the impact of different environmental conditions on signal attenuation, feature sets can be extracted separately for different weather conditions. In this paper, sunny climate is selected as a typical weather extracting signal features and designing localization algorithm. To this end, under a clear weather, typical features are extracted from a road-scale HetNet signal sequence to form a feature set vector  $e_{r_i}$ , which is expressed as follows:

$$e_{r_i} = [\overline{g_1^2}, \dots, \overline{g_K^2}, \mu_1, \dots, \mu_K, \sigma_1, \dots, \sigma_K, \overline{\Delta}_1, \dots, \overline{\Delta}_K, \chi_1, \dots, \chi_K]^T. \quad (10)$$

The feature number of the  $e_{r_i}$  is  $qK$ , where  $q$  represents the number of feature kinds. The feature descriptions of the  $K$ th BS signals in  $e_{r_i}$  are shown as Table II.

TABLE II: Feature Description

Notation	Physical meaning
$\overline{g_K^2}$	The signed mean square gradient feature
$\mu_K$	The mean RSS feature
$\sigma_K$	The RSS variance feature
$\overline{\Delta}_K$	The average difference between two BS RSSs
$\chi_K$	The RSS range feature

To theoretically analyze that localization errors can be reduced by matching multiple features, the CRLBs under different feature numbers are derived. The CRLB of one signal feature, i.e., the signed mean square gradient feature  $\overline{g^2}$ , is denoted as  $\text{CRLB}_{\overline{g^2}}$ , while  $\text{CRLB}_{\mu, \overline{g^2}}$  represents the CRLB of two signal features, i.e., the signed mean square gradient feature  $\overline{g^2}$  and the mean RSS feature  $\mu$ .

**Proposition 2:** In the segment positioning process, the error of matching multiple features is smaller than the error

of matching a single gradient feature, i.e.,  $\text{CRLB}_{\mu, \overline{g^2}} < \text{CRLB}_{\overline{g^2}}$ .

*Proof:* Please refer to Appendix C. ■

As derived in Proposition 2, the CRLB only using one signal feature, i.e., the signed mean square gradient, is  $\text{tr}(\text{CRLB}_{\overline{g^2}}) \geq \frac{\ln^2 10}{\frac{4 \cdot 10^4}{(N_l - 1)^2} \sum_{k=1}^K \frac{\beta_k^4}{\rho_k^2} (\frac{1}{d_{N_l, k}} - \frac{1}{d_{1, k}} \frac{1}{N_l})^2}$ .

Supposed that the mean RSS feature exists differences among segments, the CRLB with both the mean square gradient and mean RSS is  $\text{tr}(\text{CRLB}_{\overline{g^2}, \mu}) \geq \frac{4 \ln^2 10}{4 \ln^2 10}$ .

Hence, the CRLB difference is  $\text{tr}(\text{CRLB}_{\overline{g^2}}) - \text{tr}(\text{CRLB}_{\overline{g^2}, \mu}) \geq \frac{4b}{a(a+b)}$ , where  $a = \frac{4^2 \cdot 10^4}{(N_l - 1)^2 \ln^2 10} \sum_{k=1}^K \frac{\beta_k^4}{\rho_k^2} (\frac{1}{d_{N_l, k}} - \frac{1}{d_{1, k}} \frac{1}{N_l})^2$  and  $b = \frac{2 \cdot 20^2}{N_l^4 \ln^2 10} \sum_{k=1}^K \frac{\beta_k^2}{\eta_k^2} (\sum_{i=1}^{N_l} \frac{i}{d_{i, k}})^2$ .

Since  $\frac{4b}{a(a+b)} > 0$ , positioning accuracy can be improved by the utilization of both the mean square gradient and mean RSS features.

Therefore, by incorporating the additional information from the mean RSS, the CRLB can be further reduced, resulting in a localization error reduction of up to  $\frac{4b}{a(a+b)}$ . Meanwhile, the complexity of positioning computations can be reduced by utilizing the feature set vector to represent a road since the feature number  $qK$  is much smaller than the number of signal sampled positions  $N_l$ , i.e.,  $qK \ll N_l$ . The theoretical analysis mentioned above can be intuitively illustrated in Fig. 3. As depicted in Fig. 3(b), the road can be partitioned into four segments, where SBS's signed mean square gradient is different between two adjacent segments. However, similar gradients may exist between two non-adjacent segments, e.g., the segment 2 and the segment 4. By matching the different mean RSS features as shown in Fig. 3(c), the non-adjacent segments with similar gradients can be localized. Therefore, more statistical features are essential to identify these segments with similar gradient features to ensure segment positioning accuracy.

2) **SF Extraction:** Since not all features have significant distinctions between positions within the same spatial scale, signal features with obvious distinctions should be extracted for position representation to reduce feature-matching complexity and localization latency. By comparing the signed mean square gradient and mean RSS of the MBS in segments 2, 3, and 4 in Fig. 3(b) and Fig. 3(c), it is obvious that the mean RSS feature can be extracted as a salient feature distinguishing these segments. The reason is that the signed mean square gradient varies little between different segments, while the mean RSS feature shows a significant difference.

To prove that the feature-matching complexity can be further reduced without compromising localization accuracy by matching SFs, Proposition 3 is proposed.  $\text{CRLB}_K$  denotes that the CRLB is derived based on  $K$  signal features, and  $\text{CRLB}_{K-1}$  represents that  $K - 1$  signal features are utilized for deriving the CRLB.

**Proposition 3:** In the positioning space of roads and segments, if the normalized signal features of the  $K$ th BS changed within  $[-\gamma, \gamma]$  between all adjacent positions, the CRLB does

not change without matching the signal feature of the  $K$ th BS. Specifically,  $\text{CRLB}_K = \text{CRLB}_{K-1}$ .

*Proof:* Please refer to Appendix D. ■

As derived in Proposition 3, by matching the SF with redundant information removed, the computational complexity can be reduced and the positioning accuracy can be ensured at the same time. Therefore, it is essential to design a method to extract SFs for quickly locating vehicles.

To extract distinctive features for position representation, we propose a SF extraction method by maximizing information gain. Specifically, a feature set vector  $e_{r_i}$  in (10) is first extracted from a road-scale signal sequence  $\phi_i$ . The potential SFs of road  $r_i$  is expressed as a vector  $\mathbf{f}_{r_i}$ , which is a subset of the feature set  $e_{r_i}$ . Then, to extract the SF vector  $\mathbf{f}_{r_i}^*$  from  $e_{r_i}$ , a SF extraction method is designed as follows:

$$\mathbf{f}_{r_i}^* = \arg \max_{\mathbf{f}_{r_i} \subseteq e_{r_i}} H(r_i) - H(r_i | \mathbf{f}_{r_i}), \quad (11)$$

where  $H(r_i)$  denotes the road information entropy of RSS values in  $\phi_i$ , and  $H(r_i | \mathbf{f}_{r_i})$  represents the road conditional entropy of the SF vector  $\mathbf{f}_{r_i}$ . The conditional entropy in (11) is expressed as follows:

$$H(r_i | \mathbf{f}_{r_i}) = - \sum_{j=1}^{N_{\mathbf{f}_{r_i}}} \sum_{i=1}^m p(r_i, \mathbf{f}_j(\phi_i)) \log p(r_i | \mathbf{f}_j(\phi_i)), \quad (12)$$

where  $p(r_i, \mathbf{f}_j(\phi_i))$  represents the joint probability of road  $r_i$  and the  $j$ th feature in the feature set  $e_{r_i}$ , and  $N_{\mathbf{f}_{r_i}}$  denotes the number of feature kinds within the SF vector  $\mathbf{f}_{r_i}$ . The number of roads in the road positioning space is represented by  $m$ .  $p(r_i | \mathbf{f}_j(\phi_i))$  in (12) is the conditional probability of road  $r_i$  based on the given feature subset  $\mathbf{f}_j(\phi_i)$ , and is expressed as

$$p(r_i | \mathbf{f}_j(\phi_i)) = \frac{p(r_i) p(\mathbf{f}_j(\phi_i) | r_i)}{p(\mathbf{f}_j(\phi_i))}. \quad (13)$$

The optimal SF vector with the maximum information gain can be extracted by exhaustive searching. These extracted salient features can accurately reflect different signal propagation environments of the LoS and the NLoS links, achieving high-precision location mapping by low-dimensional features. Moreover, positioning errors caused by signal fluctuations at a single location can be mitigated by SFs since these features are extracted from multiple signal sampling positions. As the vehicle moves, the propagation environments of LoS and NLoS signals continuously change, resulting in the detection of new signals while older signals may be lost. By the proposed SF extraction method, the differences between detected signals are employed as beneficial factors that can be effectively utilized to enhance positioning accuracy.

The extracted SFs are based on path loss and slow fading models, which can represent signal propagation distance and environment on a large scale, thereby enabling precise mapping of vehicle multi-scale locations. On the other hand, due to weather variations and the movement of obstacles, the signals may rapidly fluctuate on a small scale caused by fast fading effects. The rapid changes of these signals over short distances and short periods introduce additional noise, which can be mitigated in the following two ways. First, in the

processes of extracting SFs, signal features from multiple BSs have been employed to avoid substantial fluctuations caused by fast-fading effects associated with a single BS. Second, the average of multiple signal measurements at a given location is utilized to obtain a reliable signal value, while conducting statistical feature analyses on the signals within a road region. Therefore, SFs extracted by our proposed method can filter noise from signal fluctuations, thereby ensuring positioning accuracy in the presence of fast fading.

3) **Sparse Feature Representation:** Since the extracted SFs vary with different roads and segments, to uniformly represent these different SFs, a sparse representation model is designed as follows:

$$\mathbf{f}_{r_i} = \mathbf{W}_{r_i} e_{r_i}, \quad (14)$$

where  $\mathbf{W}_{r_i} \in \mathbb{R}^{qK \times qK}$  represents a feature selection matrix that is denoted by a  $qK \times qK$  diagonal matrix, and  $qK$  represents the total number of features in the feature set vector  $e_{r_i}$ . The subscript of  $\mathbf{W}_{r_i}$  denotes that this feature extraction matrix corresponds to the road  $r_i$ . In (14),  $w_{kk}$  ( $k \in [1, qK]$ ) represents the selection coefficient of the  $k$ th feature, which is defined as a binary variable, i.e.,  $w_{kk} = 1$  if the  $k$ th feature of  $e_{r_i}$  is a SF. Otherwise,  $w_{kk} = 0$ . Since the SF vector can be represented by multiplying the feature selection matrix and the feature set vector, a vector composed of all road-scale SFs is defined as  $\mathbf{f}_r$ , which is expressed as follows:

$$\mathbf{f}_r = [\mathbf{f}_{r_1}, \dots, \mathbf{f}_{r_m}], \quad (15)$$

where  $\mathbf{f}_{r_i}$  denotes the SF vector of the road  $r_i$ , and  $\mathbf{f}_{r_i}$  is sparsely represented by  $\mathbf{W}_{r_i} e_{r_i}$ .

Since similar gradients may exist in some non-adjacent segments, e.g., the segment 2 and the segment 4 in Fig. 3(b), more statistical features with differences can be extracted to represent segments, e.g., mean RSS values showing in Fig. 3(c). Therefore, to improve the representation precision, SFs of segments can be selected by the proposed SP extraction method. To this end, the SF vector  $\mathbf{f}_{s_j}$  of the  $j$ th segment  $s_j$  on the road  $r_i$  can be extracted from corresponding feature set vector  $e_{s_j}$  through the proposed SF extraction method. Based on the proposed sparse representation model, the extracted  $\mathbf{f}_{s_j}$  can be expressed as  $\mathbf{W}_{s_j} e_{s_j}$ , where  $\mathbf{W}_{s_j} \in \mathbb{R}^{qK \times qK}$  denotes the feature selection matrix of the  $j$ th segment  $s_j$ . Then, a vector composed of all segment-scale SFs is defined as  $\mathbf{f}_s$  that takes the form of:

$$\mathbf{f}_s = [\mathbf{f}_{s_1}, \dots, \mathbf{f}_{s_{n_i+1}}], \quad (16)$$

where  $\mathbf{f}_{s_j}$  is sparsely represented as  $\mathbf{W}_{s_j} e_{s_j}$ , and  $n_i + 1$  is the number of the segments within road  $r_i$ .

### C. Coordinate Mapping

To obtain a more fine-grained position of the vehicle within a segment, curve fitting is employed to map HetNet signals into two-dimensional coordinates. Specifically,  $2K$  polynomial curve functions are utilized, where  $K$  represents the number of HetNet BSs. The longitude curve function and the latitude curve function of the  $k$ th HetNet BS within the  $l$ th segment can be expressed as follows:

$$x_j^l = G_k^l(P_{j,k}^l) = \theta_{0,k}^l + \theta_{1,k}^l P_{j,k}^l + \dots + \theta_{w,k}^l (P_{j,k}^l)^w, \quad (17)$$



$$y_j^l = H_k^l(P_{j,k}^l) = \alpha_{0,k}^l + \alpha_{1,k}^l P_{j,k}^l + \dots + \alpha_{w,k}^l (P_{j,k}^l)^w, \quad (18)$$

where  $\theta_{w,k}^l$  and  $\alpha_{w,k}^l$  ( $w \in [1, W]$ ,  $k \in [1, K]$ ,  $l \in [1, n_i + 1]$ ) respectively denote the fitted longitude and latitude coefficients. In (17) and (18),  $w$  represents the order of a polynomial,  $k$  denotes the BS index, and  $l$  is the segment index. In (17) (and (18)),  $x_j^l$  (and  $y_j^l$ ) denotes the real longitude (and latitude) of the  $j$ th position on a road.  $G_k^l(P_{j,k}^l)$  (and  $H_k^l(P_{j,k}^l)$ ) is the estimated longitude (and latitude) based on the RSSs of the  $k$ th BS. The coefficients of (17) and (18) are determined by the least squares principle described in [42] to minimize fitting errors. The final longitude and latitude results are obtained by the average longitude and latitude values mapped by all HetNet RSS values, respectively.

## V. MULTI-SCALE VEHICLE LOCALIZATION

To locate a vehicle dynamically, the vehicular SFs are first extracted from the real-time HetNet signal sequence using the sparse representation model. Then, by integrating inclusion and adjacency relationships between roads and segments, we propose the MSVL algorithm to locate the vehicular road, segment, and coordinate based on extracted SFs.

### A. Real-time Signal Feature Extraction

To extract real-time SFs, the vehicular HetNet signal sequence of a segment is first acquired by SPs extracted in Section IV-A. Then, the vehicular feature set vector  $e_u$  can be extracted by the model in (10) from the real-time HetNet signal sequence. The vehicular multi-scale SF vectors, i.e.,  $\hat{\mathbf{f}}_{r_i}$  and  $\hat{\mathbf{f}}_{s_l}$ , can be extracted by multiplying the vehicular feature set vector and the feature selection matrix of the matched road  $r_i$  and segment  $s_l$ .

### B. Multi-scale Feature Matching

To achieve high precision with low computation complexity, the posterior probability of a segment is utilized for vehicular localization by fusing geographical prior information. Based on the road feature vector  $\mathbf{f}_r$  and segment feature vector  $\mathbf{f}_s$ , the vehicular posterior probability of a segment can be obtained by applying the Bayes' rule as follows:

$$\begin{aligned} \Pr(\hat{s}_l | s_l) &= \Pr(\hat{\mathbf{f}}_{s_l} | \mathbf{f}_{s_l}) \\ &= \frac{\Pr(\hat{\mathbf{f}}_{r_i} | \mathbf{f}_{r_i}) \Pr(s_l | r_i) \Pr(\hat{\mathbf{f}}_{s_l})}{\sum_{q=1}^{n_i+1} \Pr(\hat{\mathbf{f}}_{s_q} | \mathbf{f}_{s_q}) \Pr(\mathbf{f}_{s_q})}, \end{aligned} \quad (19)$$

where  $\Pr(\hat{\mathbf{f}}_{r_i} | \mathbf{f}_{r_i})$  denotes the matching probability of road-scale SFs,  $\Pr(\hat{\mathbf{f}}_{s_l} | \mathbf{f}_{s_l})$  and  $\Pr(\hat{\mathbf{f}}_{s_q} | \mathbf{f}_{s_q})$  represent the matching probability of different segment-scale SFs. In the (19),  $\Pr(s_l | r_i)$  denotes the prior probability of the segment  $s_l$  within the road  $r_i$ .

Based on the posterior probability  $\Pr(\hat{s}_l | s_l)$ , the segment localization problem can be formulated as follows:

$$\hat{s}_l = \arg \max_{s_l \in \mathcal{S}_i} \Pr(\hat{s}_l | s_l), \quad (20)$$

To locate the vehicular positions with the highest posterior probability, we propose the MSVL algorithm which includes three modules, i.e., the road recognition module, the segment positioning module, and the coordinate localization module.

1) **Road recognition module:** To recognize the real-time road SFs from the road-scale SF vector  $\mathbf{f}_r$ , the vehicular SFs are matched with and each road SFs to maximize the road feature-matching probability. The road feature-matching probability  $\Pr(\hat{\mathbf{f}}_{r_i} | \mathbf{f}_{r_i})$  fits to an exponential probability distribution [43] that can be expressed as:

$$\Pr(\hat{\mathbf{f}}_{r_i} | \mathbf{f}_{r_i}) = e^{-d(\hat{\mathbf{f}}_{r_i}, \mathbf{f}_{r_i})}, \quad (21)$$

where  $d(\hat{\mathbf{f}}_{r_i}, \mathbf{f}_{r_i})$  represents the  $l_2$ -norm between the vector of vehicular SFs and the vector of  $j$ th road-scale SFs in  $\mathbf{f}_{r_i}$ . The  $l_2$ -norm  $d(\hat{\mathbf{f}}_{r_i}, \mathbf{f}_{r_i})$  can be obtained as follows:

$$d(\hat{\mathbf{f}}_{r_i}, \mathbf{f}_{r_i}) = \|\mathbf{W}_{r_i} e_u - \mathbf{W}_{r_i} e_{r_i}\|_2, \quad (22)$$

where  $\mathbf{W}_{r_i} e_{r_i}$  denotes the  $j$ th road's SFs in the road-scale SF vector  $\mathbf{f}_r$ , and  $\mathbf{W}_{r_i} e_u$  represents the vehicular SFs corresponding to the  $j$ th road. With the highest probability of road-scale feature matching, real-time information about the vehicular road can be obtained.

2) **Segment positioning module:** To identify the specific location of the vehicular segment within the located road, the vehicular segment SFs are compared with the SFs in  $\mathbf{f}_s$  maximizing segment posterior probability. The probability of segment feature matching  $\Pr(\hat{\mathbf{f}}_{s_l} | \mathbf{f}_{s_l})$  can be given by:

$$\Pr(\hat{\mathbf{f}}_{s_l} | \mathbf{f}_{s_l}) = e^{-d(\hat{\mathbf{f}}_{s_l}, \mathbf{f}_{s_l})}, \quad (23)$$

where  $d(\hat{\mathbf{f}}_{s_l}, \mathbf{f}_{s_l})$  represents the  $l_2$ -norm between the vector of vehicular segment SFs and the vector of the  $l$ th SFs in  $\mathbf{f}_s$ . The  $d(\hat{\mathbf{f}}_{s_l}, \mathbf{f}_{s_l})$  can be expressed as follows:

$$d(\hat{\mathbf{f}}_{s_l}, \mathbf{f}_{s_l}) = \|\mathbf{W}_{s_l} e_u - \mathbf{W}_{s_l} e_{s_l}\|_2, \quad (24)$$

where  $\mathbf{W}_{s_l} e_{s_l}$  represents the vehicular SFs. In (24),  $\mathbf{W}_{s_l} e_{s_l}$  denotes the SF vector of the  $l$ th segment in the  $\mathbf{f}_s$ . By road and segment joint feature matching, the vehicular segment can be quickly located with the maximum segment posterior probability.

3) **Coordinate localization module:** After acquiring the road and the segment by the road recognition module and the segment positioning module, the  $j$ th coordinate within the determined segment, i.e.,  $\hat{\mathbf{c}}_j = [\hat{x}_j^l, \hat{y}_j^l]^\top$  can be acquired as follows:

$$\hat{x}_j^l = \frac{1}{K} \sum_{k=1}^K G_k^l(P_{j,k}^l), \quad (25)$$

$$\hat{y}_j^l = \frac{1}{K} \sum_{k=1}^K H_k^l(P_{j,k}^l), \quad (26)$$

where  $\hat{x}_j^l$  and  $\hat{y}_j^l$  denote the estimated longitude and latitude values.  $G_k^l(P_{j,k}^l)$  and  $H_k^l(P_{j,k}^l)$  represent the fitted curves obtained by (17) and (18) based on the  $k$ th BS signals. Subsequently, the multi-scale localization problem in (3) can be solved, and the real-time vehicular position  $\mathbf{p} = [\hat{x}, \hat{s}_l, \hat{\mathbf{c}}_j]^\top$  can be localized with low latency and high precision.

In the proposed MSVL algorithm, the highest computation complexity occurs when each road and segment is represented by all features of the feature set. The highest computation complexity is  $\mathcal{O}(qK(m+n_i+1))$ , where  $m$ ,  $n_i+1$ , and  $qK$  represent the number of roads, the number of segments within the localized road, and the number of feature kinds in the feature set, respectively. As the number of feature kinds  $q$  increases, the localization latency will correspondingly increase. This is because the computational cost of the proposed MSVL algorithm is linearly related to the number of features. With the increase in the feature number, the algorithm will need to process larger amounts of data, leading to an increase in computation time. Therefore, in practical applications, salient feature extraction is crucial to extract sparse features reducing computation complexity, and balancing mechanism positioning accuracy and positioning delay.

---

### Algorithm 1 MSVL Algorithm

---

**Input:** The road-scale SF vector  $\mathbf{f}_r$ , the segment-scale SF vector  $\mathbf{f}_s$ , the real-time HetNet signal sequence  $\{\mathbf{o}_1, \dots, \mathbf{o}_t\}$ , the vehicular feature set vector  $\mathbf{e}_u$ .

**Output:** The estimated road  $\hat{r}_i$ , segment  $\hat{s}_l$ , and the real-time coordinate  $\hat{\mathbf{c}}$ .

- 1:  $\hat{r}_i \leftarrow \phi$ ,  $\hat{s}_l \leftarrow \phi$ ,  $\hat{\mathbf{c}} = [\hat{x}, \hat{y}]^\top \leftarrow \phi$ ;
- 2: The road matching probability set  $\mathcal{D}_{r_i} \leftarrow \phi$ ;
- 3: The segment posterior probability set  $\mathcal{D}_{s_l} \leftarrow \phi$ ;
- 4: **for**  $\mathbf{f}_{r_i}$  in  $\mathbf{f}_r$  **do**
- 5:     Based on the Proposition 2 and the Proposition 3, extract the vehicular road-scale SFs  $\hat{\mathbf{f}}_{r_i}$ ;
- 6:     The road matching probability  $\Pr(\hat{\mathbf{f}}_{r_i} | r_i)$ ;
- 7:      $\mathcal{D}_{r_i} \leftarrow \mathcal{D}_{r_i} \cup \Pr(\hat{\mathbf{f}}_{r_i} | r_i)$ ;
- 8: **end for**
- 9: The vehicular road  $\hat{r}_i$  with the maximum  $\Pr(\hat{\mathbf{f}}_{r_i} | r_i)$ ;
- 10: **for**  $\mathbf{f}_{s_l}$  in  $\mathbf{f}_s$  of the road  $r_i$  **do**
- 11:     The vehicular segment-scale SFs  $\hat{\mathbf{f}}_{s_l}$ ;
- 12:     The segment posterior probability  $\Pr(s_l | \hat{\mathbf{f}}_{s_l})$ ;
- 13:      $\mathcal{D}_{s_l} \leftarrow \mathcal{D}_{s_l} \cup \Pr(s_l | \hat{\mathbf{f}}_{s_l})$ ;
- 14: **end for**
- 15: The vehicular segment  $\hat{s}_l$  with the maximum  $\Pr(s_l | \hat{\mathbf{f}}_{s_l})$ ;
- 16: The vehicular coordinate  $\hat{\mathbf{c}} = [\hat{x}, \hat{y}]^\top$  within the positioned segment  $\hat{s}_l$ ;
- 17: **return** The vehicular road  $\hat{r}_i$ , the segment  $\hat{s}_l$ , and the real-time coordinate  $\hat{\mathbf{c}}$ ;

---

The pseudo-code of the multi-scale vehicular localization process is presented in algorithm 1. The inputs of algorithm 1 are the multi-scale feature vector, a real-time vehicular RSS sequence, and the vehicular feature set vector. First, the vehicular road is located by SF matching between the vehicular road-scale SF vector and the extracted road-scale feature vector (steps 1-9). Then, the vehicular segment is located by maximizing the segment posterior probability based on SF matching (steps 10-15). Finally, the vehicular real-time coordinate within the located segment can be positioned through curve fitting (step 16). The outputs of algorithm 1 are the vehicular moving road, segment, and the real-time vehicular coordinate (step 17).

## VI. EXPERIMENT RESULTS AND ANALYSIS

In this section, we conduct experiments to evaluate the localization performance of the proposed multi-scale localization mechanism, and the results are compared in terms of segment positioning error, coordinate positioning error, and coordinate mean localization latency.

### A. Simulation Setup

The simulations are conducted in the Python 3.9 on a PC with 24 GB RAM. Unless otherwise stated, the system parameters are set as follows. The number of feature kinds  $q$  in the proposed mechanism is set as 5. Signals of 6 HetNet BSs are used for vehicle localization, i.e., the maximum  $K$  is equal to 6. The distance interval of signal sampling  $\Delta D$  is set as 1 m. The sampling interval time  $t$  and the vehicular speed  $v$  are respectively set as 125 ms and 30 Km/h for signal collecting and real-time positioning simulation.

In the conducted experiments, the proposed mechanism is evaluated within a HetNet utilizing the 4G frequency band ranging from 1800 MHz to 1900 MHz and the 5G frequency band spanning 3400 MHz to 3600 MHz. Specifically, to accurately reflect the path loss in the 4G mobile systems, the Cost-231 Hata model [44] is used to model the 4G channels based on the frequency band between 1800MHz and 1900MHz. This model can effectively incorporate urban architectural influences considering factors such as street widths, heights of surrounding buildings, and their spatial distribution, and allow for application across diverse environments, including urban, suburban, and rural settings. Meanwhile, the 1800MHz to 1900MHz frequency band in 4G has a higher signal transmission rate suitable for urban areas and densely populated places of vehicle positioning. Then, the 5G path loss model for our proposed mechanism is developed in alignment with TR 38.901 [45] operating on the frequency band between 3400MHz to 3600MHz, where various channel models tailored for diverse scenarios, including train, vehicle, urban, and rural environments can be outlined.

Four approaches are implemented for performance comparison, i.e., the state of art restricted weighted K-nearest neighbor algorithm (RWKNN) [46], the hierarchical localization method (HLM) [47], the gradient-based fingerprinting (GIFT) [48], and the curve fitting-based exhaustive location search algorithm (CF-ELS) [42]. The former two methods are compared since they respectively utilize uniform grid signals and hierarchical signals to locate vehicles. The GIFT is chosen due to VUE can be located through gradient feature matching. The CF-ELS is chosen to be compared as range estimations are utilized in VUE localization. The number of nearest neighbors is set as 3 in RWKNN [46]. Two hidden layer sizes of the auto-encoder applied in HLM are set as 100 and 6, respectively [47]. The step size of the exhaustive search in CF-ELS is set to 0.1 m [42].

To evaluate that the positioning performance in wide localization environments, an interested area of 0.6 Km  $\times$  0.6 Km was established by the Qualnet simulator based on real service parameters of HetNet BSs [49], as shown in Fig. 4. There are 1 MBS and 5 SBS in the localization scenario. Building 1 is

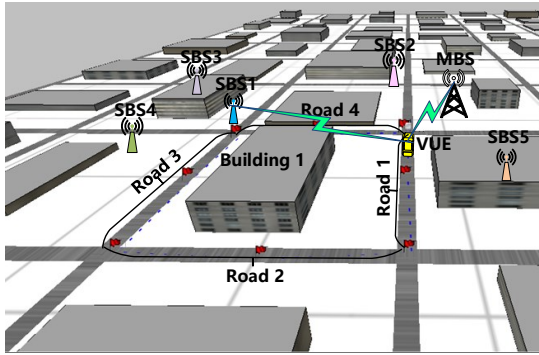


Fig. 4: Localization scenario in the Qualnet simulator.

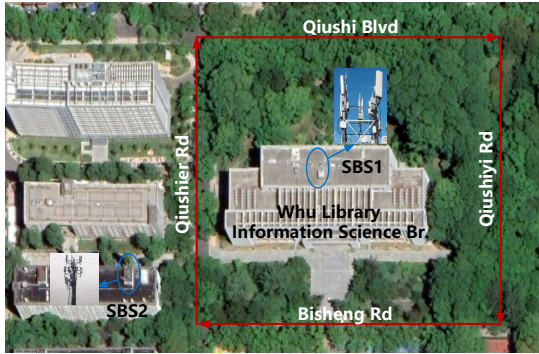


Fig. 5: Localization scenario in an urban environment.

an urban high-rise building and its height is 65 m. The width of each road in Fig. 4 is 20 m. To further verify the positioning performance of the road-aware positioning mechanism in real road environments, a real-world area of 0.15 Km  $\times$  0.15 Km was selected at Wuhan University, as shown in Fig.5. The vehicular positions are estimated when the vehicle moves around building 1 along four roads as shown in Fig. 4. In the real-world urban road environment, the vehicle will be located while moving on the four roads as shown in Fig.5.

To assess the effectiveness of the proposed mechanism and the benchmark methods in terms of localization, both simulated and real experiments are conducted by extracting the simulated data set and the real-world data set, respectively. Specifically, the simulation data set was collected by signal measurement reports in the Qualnet simulator, with 13932 records obtained from the targeted localization area. In the simulation data set, each record contains RSS values from 6 HetNet BSs along with a 2D coordinate. In the real experiments, we collect the real-world data set along different roads through the Great Scott Gadget HackRF [23], which can be able to capture radio signals from 1 MHz to 6 GHz and whose signal sensitivity can reach as low as -120 dBm. This real-world data set contains 6495 records, where each record contains a two-dimensional coordinate and RSS values from 2 HetNet BSs. In the real-time vehicle positioning stage, the VUE received signals can be extracted by an RF measurement tool (Cellular-Z) [50].

### B. Segment Positioning Performance

In Fig. 6, the root mean squared error (RMSE) is simulated with the increasing SNR of the service BS to evaluate the

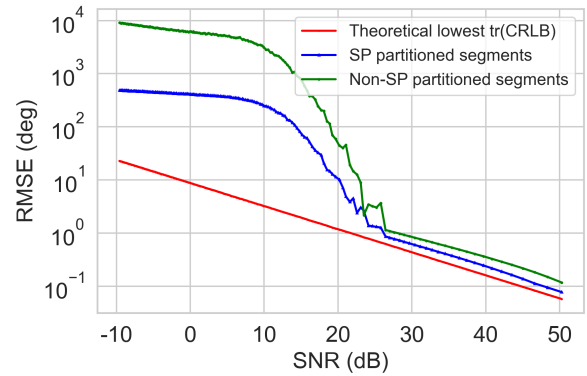


Fig. 6: RMSE of different partitioning segments.

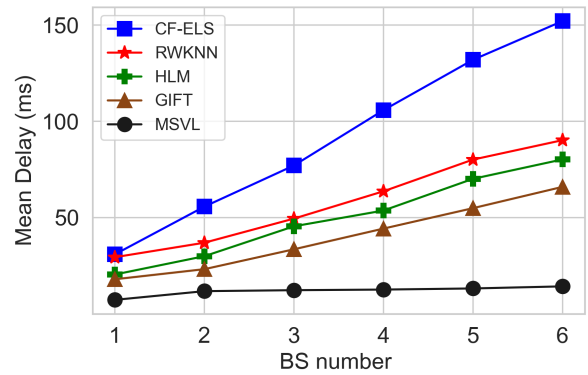


Fig. 7: Mean delay versus BS number.

effectiveness of the proposed SP segmentation method. The SNR is defined as  $SNR = 10 \log \frac{\sigma_{Signal}^2}{\sigma_{Noise}^2}$ , where  $\sigma_{Signal}^2$  and  $\sigma_{Noise}^2$  respectively are the signal variance and the noise variance. The SP partitioned segments are obtained using the proposed SP segmentation method based on the Proposition 1 and Remark 1. The non-SP partitioned segments are divided by the signals are not the extreme points and turning points of a HetNet signal sequence. In Fig. 6, the RMSE of the segments positioned by SPs can approach the lowest CRLB as the SNR increases, indicating that SP partitioned segments are more resistant to noise during the positioning process. The result in Fig. 6 also demonstrates that the proposed sequence segmentation method can accurately partition segments and indeed reduce the segment localization error.

### C. Coordinate Positioning Performance

Since the detectable BS number and the grid size play crucial roles in accurate signal feature extraction and computation complexity, simulation experiments were conducted to investigate the impact of these two parameters on the mean delay and the mean distance error (MDE). The mean delay is calculated by  $\bar{T} = \frac{1}{N_l} \sum_{i=1}^{N_l} T_i$ , and the MDE is defined

as  $MDE = \frac{1}{N_l} \sum_{i=1}^{N_l} \Delta E_i$ , where  $T_i$  and  $\Delta E_i$  respectively denote the localization latency and the localization error of the  $i$ th position.  $N_l$  represents the number of estimated target positions within the  $l$ th segment.

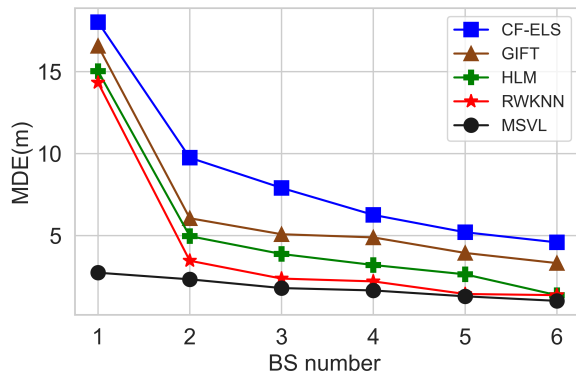


Fig. 8: Mean error versus BS number.

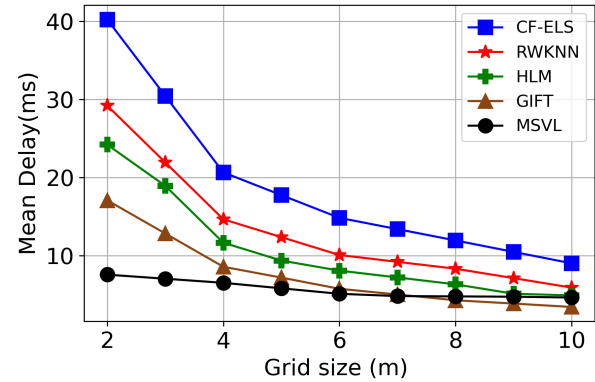


Fig. 10: Mean delay versus grid size.

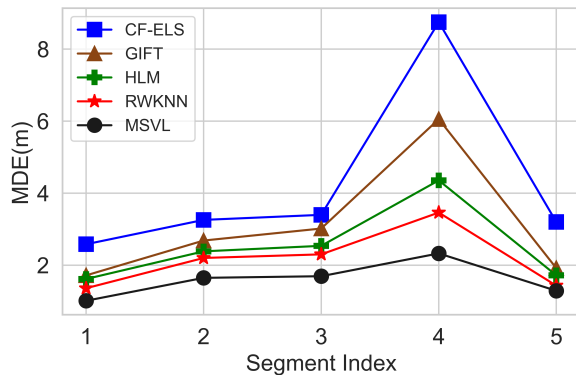


Fig. 9: MDE of different segments with varying BS number.

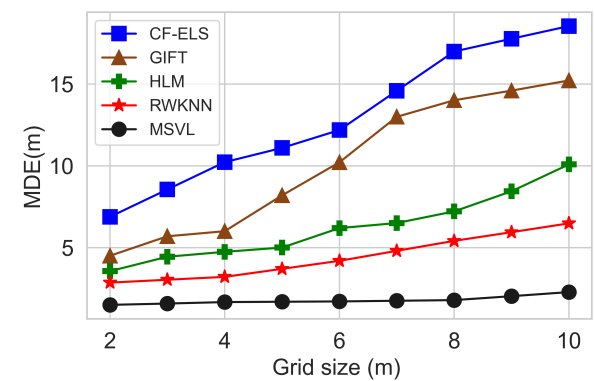


Fig. 11: Mean error versus grid size.

1) *Impact of the HetNet BS number:* In Figs. 7 and 8, the vehicular mean delay and the MDE of coordinate positions are illustrated respectively under different HetNet BS numbers at the grid size of 2 m for the proposed multi-scale localization mechanism and benchmark schemes. Specifically, it can be observed from Fig. 7 that the proposed mechanism achieves the lowest mean delay compared with the benchmark method. This is due to the significantly reduced computation complexity, achieved by the utilization of low-dimension road and segment positioning space, as well as the sparse SFs in the feature-matching localization. The effect of the different BS numbers on the MDE of the proposed mechanism outperforms benchmark methods is shown in Fig. 8. It is observed from Fig. 8 that the proposed mechanism can achieve a minimum MDE of 2.43 m when VUE receives signals from 2 BSs, owing to the substantial signal attenuation in the 5G HetNet. Since the RWKNN, HLM, GIFT, and CF-ELS methods are respectively based on uniform grids, dual-layer fingerprints, single gradient features, and triangulation positioning, these methods exhibit higher latency or positioning errors under different BS numbers.

To evaluate the localization performance of our proposed mechanism in large environments, the experiment of localization error under different BS numbers is conducted. As shown in Fig. 9, a vehicle was moving on a road from the segment 1 to the segment 5, which is represented by segment indexes. The detected BS numbers of the segment 1 to the segment 5 are 6, 4, 4, 2, and 5, respectively. It can be seen that when

the vehicle moves on the segment 4 which can only detect a MBS and a SBS, the MDEs of the benchmark methods are larger than the MDE of the proposed mechanism. This is because we mainly utilize the different properties of HetNet BSs rather than rely on absolute signal values.

2) *Impact of Different Grid Sizes:* In Figs. 10 and 11, we show the mean delay and the MDE of coordinate positions under different grid sizes for the proposed multi-scale localization mechanism and benchmark schemes, respectively. Fig. 10 shows that the mean delay decreases as the grid size increases. Specifically, the lowest mean delay is achieved by the proposed mechanism at the smallest grid size of 2 m, measuring less than 10 ms. The reason is that roads and segments are divided according to the actual length of the road and HetNet signal features, thereby avoiding reliance on uniform grid sizes. Meanwhile, MDE of the proposed algorithm gradually decreases as the grid size increases and remains below 2.5 m, as depicted in Fig. 11. Since the RWKNN, HLM, GIFT, and CF-ELS methods rely on uniform grids for signal feature extraction and vehicle localization, the MDEs of benchmark methods would increase as the grid size increases. In contrast, the proposed mechanism can achieve low-latency and high-precision vehicle localization under large grid sizes.

Based the above simulations of grid size on positioning latency and accuracy, the following analysis is provided regarding the sampling interval and vehicle speed that determine the grid size. To obtain a minimum grid of 1 m for evaluating

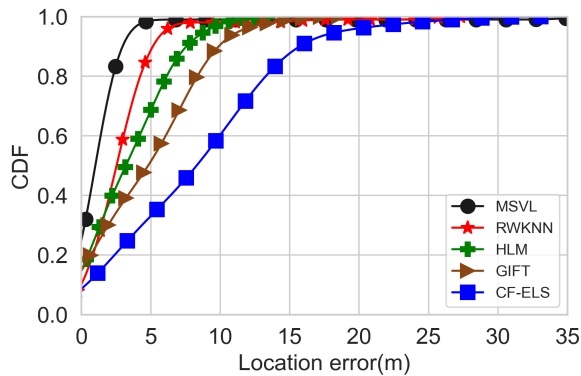


Fig. 12: CDF based on simulated signal measurements.

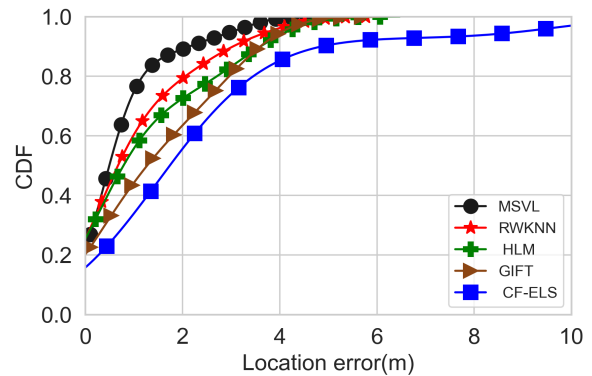


Fig. 13: CDF based on real signal measurements.

positioning performance, the signal sampling time interval and vehicle speed were set to 125 ms and 30 Km/h, respectively. Under the constant sampling time interval  $t$ , increasing vehicle speed  $v$  may reduce localization accuracy in signal collection and real-time positioning processes. The reason is that higher speeds accentuate the Doppler effect, resulting in carrier frequency offsets and rapid fading of received wireless signals, which distorts signal features. Moreover, larger sampling intervals may result in the loss of critical information, further diminishing localization precision. Doppler compensation methods [51] and lower signal sampling time intervals can be used to solve the above issues for maintaining accurate positioning. When the vehicle speed remains constant, an increase in the signal sampling time interval results in a larger sampled distance interval. This leads to incorrectly partitioning of signal segments and inaccuracies in segment-scale features, ultimately diminishing the positioning accuracy of the proposed mechanism. Therefore, a small signal sampling time interval is utilized for maintaining precise signal representation and overall mechanism performance.

Fig. 12 shows the cumulative distribution function (CDF) of localization errors using 2 HetNet BSs at the 2 m grid size. The proposed multi-scale vehicle localization algorithm achieves improvements of 25%, 33%, 45%, and 77% (from 2.6 m to 0 m) compared to RWKNN, HLM, GIFT, and CF-ELS in terms of distance estimation error.

To intuitively reflect the real-time positioning process of vehicles through our mechanism in HetNet, we have made the experimental process into a short movie [52]. In this movie, a vehicle is positioned by our proposed mechanism in a crowded urban road environment. The real-time HetNet signals and their associated features are first extracted. Then, the proposed MSVL algorithm is employed to determine roads, segments, and coordinates, ensuring accurate navigation within complex urban road environments.

3) *Performance Comparison under the Real Data Set:* To conduct real experiments on vehicle positioning in urban road environments, the CDF of localization errors are evaluated based on the real-world data set collected from a HetNet scenario. It can be seen from Fig. 13 that our proposed algorithm shows a 17%, 21%, 27%, and 35% improvement (from 2 m to 0 m) respectively compared to RWKNN, HLM, GIFT, and CF-ELS.

Table III depicts the mean delay of the four localization methods using the real-world data set. As the searching space is divided into the road searching space and the segment searching space, our proposed method's mean delay could be reduced to 7.2 ms. For high-speed vehicles, a localization delay under 10 ms is crucial for maintaining a safe distance between vehicles [53]. Given that the localization times of RWKNN, HLM, GIFT, and CF-ELS exceed 10 ms, meeting the vehicle localization requirements with low latency and high reliability becomes challenging.

TABLE III: Mean delay of located positions

Method	RWKNN	HLM	GIFT	CF-ELS	MSVL
Mean delay (ms)	32.7	30.1	28.5	57.8	7.2

In the above simulation experiments, the localization performance of the MSVL algorithm can achieve low latency and high precision in single-lane environments. In multi-lane road environments, localization errors of our proposed mechanism can be reduced by increasing BS density and road infrastructures. Specifically, through increasing BS density, more BS signals with differences can be utilized to locate vehicles, thereby reducing localization errors. In the field of intelligent transportation, to achieve low-latency and high-reliability vehicle positioning, more road side communicating and sensing infrastructures can be constructed for lane-level positioning and automatic driving.

## VII. CONCLUSIONS

In this paper, we proposed a multi-scale localization mechanism achieving low-latency vehicle localization. Specifically, a SP segmentation method and a SF extraction method were devised to sparsely represent roads and segments. Then, a MSVL algorithm was proposed through road and segment SF matching. Fine-grained positioning was achieved through curve fitting to localize vehicular coordinates. The numerical results confirmed that our proposed mechanism offers a promising solution to reduce localization latency and support reliable localization accuracy. The impact of faint HetNet signal variations on the localization performance of the proposed mechanism is a potential concern. However, this issue can be



addressed by utilizing the different signals from more HetNet BSs. As part of future work, with the help of high precision beam forming, accurate lane-level positioning can be achieved by aiming the BS beam at the lane and then extracting lane-level signal features.

#### APPENDIX A: DETAILED CALCULATION OF CRLB

To locate the  $l$ th segment, suppose distance interval of signal sampling is 1 m, i.e.,  $\Delta D = \sqrt{(x_{k+1}^l - x_k^l)^2 + (y_{k+1}^l - y_k^l)^2} = 1$  m, the mean square gradient feature of the  $k$ th BS RSSs within the  $l$ th segment in (1) can be expressed as follows:

$$\overline{g_k^l} = \frac{(10\beta_k^l)^2}{N_l - 1} \sum_{i=1}^{N_l-1} (\log d_{i+1,k}^l - \log d_{i,k}^l)^2 + Z_k^l, \quad (27)$$

where  $d_{i,k}^l$  is the distance between the  $i$ th position in the segment and the position of the  $k$ th BS.  $d_{i,k}^l$  is calculated by the Euclidean distance as follows:

$$d_{i,k}^l = \sqrt{(x_i^l - x_{BS_k})^2 + (y_i^l - y_{BS_k})^2}, \quad (28)$$

where  $x_i^l$  and  $y_i^l$  respectively represent the longitude value and the latitude value of the  $i$ th position within the  $l$ th segment.  $x_{BS_k}$  and  $y_{BS_k}$  respectively represent the longitude value and the latitude value of the  $j$ th BS. To find the coordinate derivative of segment positioning, coordinates within the  $l$ th segment are mapped to the middle position as follows:

$$x_i^l = \frac{2i}{N_l}(x_m^l - x_1^l) + x_1^l, \quad (29)$$

$$y_i^l = \frac{2i}{N_l}(y_m^l - y_1^l) + y_1^l, \quad (30)$$

where  $x_m^l$  and  $y_m^l$  respectively represent the longitude value and latitude value of the middle position in the  $l$ th segment. And  $x_1^l$  and  $y_1^l$  are the 2D coordinate of the first position in the  $l$ th segment. The Jacobian matrix of all BSs measurement errors evaluated at the true segment  $\mathbf{c}_m^l = [x_m^l, y_m^l]^T$  takes the form

$$J_{g^2} = \begin{pmatrix} \frac{\partial \overline{g_1^l}}{\partial x_m^l} & \frac{\partial \overline{g_1^l}}{\partial y_m^l} \\ \vdots & \vdots \\ \frac{\partial \overline{g_K^l}}{\partial x_m^l} & \frac{\partial \overline{g_K^l}}{\partial y_m^l} \end{pmatrix}. \quad (31)$$

The derivative of the mean square gradient feature can be expressed by

$$\frac{\partial \overline{g_k^l}}{\partial x_m^l} = \frac{(10\beta_k^l)^2}{(N_l - 1) \ln 10} \left[ \sum_{i=1}^{N_l-1} 2 (\log d_{i+1,k}^l - \log d_{i,k}^l) \right. \quad (32)$$

$$\left. \left( \frac{\cos \theta_{i+1,k}^l}{d_{i+1,k}^l} \frac{2(i+1)}{N_l} - \frac{\cos \theta_{i,k}^l}{d_{i,k}^l} \frac{2i}{N_l} \right) \right],$$

$$\frac{\partial \overline{g_k^l}}{\partial y_m^l} = \frac{(10\beta_k^l)^2}{(N_l - 1) \ln 10} \left[ \sum_{i=1}^{N_l-1} 2 (\log d_{i+1,k}^l - \log d_{i,k}^l) \right. \quad (33)$$

$$\left. \left( \frac{\sin \theta_{i+1,k}^l}{d_{i+1,k}^l} \frac{2(i+1)}{N_l} - \frac{\sin \theta_{i,k}^l}{d_{i,k}^l} \frac{2i}{N_l} \right) \right],$$

where  $\theta_{i,k}^l$  is the azimuth angle between the  $i$ th position and the  $k$ th BS within the  $l$ th segment. The noise covariance matrix of the mean square gradient feature is

$$\Sigma_{g^2} = \text{diag}[\rho_1^l, \dots, \rho_K^l]_{N_l \times N_l}. \quad (34)$$

The Fisher information matrix (FIM) and the corresponding CRLB of all BSs' measurements take the form

$$\Phi = J_{g^2}^T \Sigma_{g^2}^{-1} J_{g^2}, \quad (35)$$

$$\text{CRLB} = \Phi^{-1}. \quad (36)$$

Since the  $\text{tr}(\text{CRLB})$  can not be smaller than the sum of the FIM's reciprocal diagonal elements, based on the inequality transformation method in [39], the optimal objective becomes

$$\arg \min_{\{d_i^l\}, i=1, \dots, N_l} \text{tr}(\text{CRLB}) \geq \frac{4}{\Phi_{11} + \Phi_{22}}. \quad (37)$$

To obtain the simplified result of  $\Phi_{11} + \Phi_{22}$ , a special situation is considered, where the VUE's trajectory and positions of all BSs are on a line. The lowest trace values of CRLB in other scenarios will be greater than the value in this scenario. In this situation,  $\cos \theta_{i+1,k}^l = \cos \theta_{i,k}^l$  and  $\sin \theta_{i+1,k}^l = \sin \theta_{i,k}^l$ . Since the signal sampling distance interval  $d_{i+1,k}^l - d_{i,k}^l = 1$  m, and there is a conversion relationship between the mean square gradient variance and the RSS variance, by plugging (31) - (35) into (37), the smallest  $\text{tr}(\text{CRLB})$  is a value related to the distances between VUE and BSs, and we have

$$\text{tr}(\text{CRLB}) \geq \frac{\ln^2 10}{\frac{4 \cdot 10^4}{(N_l - 1)^2} \sum_{k=1}^K \frac{\beta_k^l{}^4}{\rho_k^l{}^2} \left( \frac{1}{d_{N_l,k}^l} - \frac{1}{d_{1,k}^l} \frac{1}{N_l} \right)^2}. \quad (38)$$

#### APPENDIX B: PROOF OF PROPOSITION 1

$C_{g^2}(d)$  is defined as the CRLB of the  $l$ th segment whose endpoints are not the signal extreme points. If the  $l$ th segment is partitioned by the signal extreme points, i.e.,  $d_{N_l,k}^l = d_{min,k}^l$  and  $d_{1,k}^l = d_{max,k}^l$ , the CRLB of this  $l$ th segment is expressed as  $C_{g^2}(d')$ . The ratio between  $C_{g^2}(d)$  and  $C_{g^2}(d')$  can be given as follows:

$$\begin{aligned} \frac{C_{g^2}(d)}{C_{g^2}(d')} &= \frac{\ln^2 10}{\frac{4 \cdot 10^4}{(N_l - 1)^2} \sum_{k=1}^K \frac{\beta_k^l{}^4}{\rho_k^l{}^2} \left( \frac{1}{d_{N_l,k}^l} - \frac{1}{d_{1,k}^l} \frac{1}{N_l} \right)^2} \times \\ &\frac{4 \cdot 10^4}{(N_l - 1)^2} \sum_{k=1}^K \frac{\beta_k^l{}^4}{\rho_k^l{}^2} \left( \frac{1}{d_{min,k}^l} - \frac{1}{d_{max,k}^l} \frac{1}{N_l} \right)^2 \\ &= \frac{\ln^2 10}{\sum_{k=1}^K \frac{\beta_k^l{}^4}{\rho_k^l{}^2} \left( \frac{1}{d_{min,k}^l} - \frac{1}{d_{max,k}^l} \frac{1}{N_l} \right)^2} \times \\ &\frac{\sum_{k=1}^K \frac{\beta_k^l{}^4}{\rho_k^l{}^2} \left( \frac{1}{d_{N_l,k}^l} - \frac{1}{d_{1,k}^l} \frac{1}{N_l} \right)^2}{\sum_{k=1}^K \frac{\beta_k^l{}^4}{\rho_k^l{}^2} \left( \frac{1}{d_{N_l,k}^l} - \frac{1}{d_{1,k}^l} \frac{1}{N_l} \right)^2}. \end{aligned} \quad (39)$$

Since the segment corresponding to  $C_{g^2}(d)$  is not partitioned by the signal extreme points, its distances of endpoints are not the extreme points as well. Thus,  $d_{N_l,k}^l > d_{min,k}^l$  and  $d_{1,k}^l < d_{max,k}^l$ . Then,  $\frac{C_{g^2}(d)}{C_{g^2}(d')} > 1$ , which proves the proposition 1.

#### APPENDIX C: PROOF OF PROPOSITION 2

The mean RSS feature of the  $k$ th BS within the  $l$ th segment can be expressed as follows:

$$\mu_k^l = \frac{1}{N_l} \sum_{i=1}^{N_l} P_{i,k}^l = \frac{-10\beta_k^l}{N_l} \sum_{i=1}^{N_l} \log d_{i,k}^l + P_{0,k}^l + W_k^l \quad (40)$$

where  $d_{i,k}^l$  is the distance between the VUE's  $i$ th position and the  $k$ th BS's position. By plugging (28) - (30) into (40), the derivative of the  $k$ th BS's mean RSS feature can be expressed by

$$\frac{\partial \mu_k^l}{\partial x_m^l} = \frac{-20\beta_k^l}{(N_l^2) \ln 10} \sum_{i=1}^{N_l} \frac{i \cos \theta_{i,k}^l}{d_{i,k}^l}, \quad (41)$$



$$\frac{\partial \mu_k^l}{\partial y_m^l} = \frac{-20\beta_k^l}{(N_l^2) \ln 10} \sum_{i=1}^{N_l} \frac{i \sin \theta_{i,k}^l}{d_{i,k}^l}. \quad (42)$$

The Jacobian matrix of the all BSs measurement errors evaluated at the true segment  $\mathbf{c}_m^l = [x_m^l, y_m^l]^T$  is

$$J_\mu = \begin{pmatrix} \frac{\partial \mu_1^l}{\partial x_m^l} & \frac{\partial \mu_1^l}{\partial y_m^l} \\ \vdots & \vdots \\ \frac{\partial \mu_K^l}{\partial x_m^l} & \frac{\partial \mu_K^l}{\partial y_m^l} \end{pmatrix} = \alpha \begin{pmatrix} \sum_{i=1}^{N_l} \frac{i \cos \theta_{i,1}^l \beta_1^l}{d_{i,1}^l} & \sum_{i=1}^{N_l} \frac{i \sin \theta_{i,k}^l \beta_1^l}{d_{i,k}^l} \\ \vdots & \vdots \\ \sum_{i=1}^{N_l} \frac{i \cos \theta_{i,K}^l \beta_K^l}{d_{i,K}^l} & \sum_{i=1}^{N_l} \frac{i \sin \theta_{i,K}^l \beta_K^l}{d_{i,K}^l} \end{pmatrix} \quad (43)$$

where  $\alpha = \frac{-20}{(N_l^2) \ln 10}$ . The measurement noise covariance matrix of the mean RSS feature is

$$\Sigma_\mu = \text{diag}[\eta_1^l, \dots, \eta_K^l]_{N_l \times N_l}. \quad (44)$$

The FIM of the mean RSS feature and the mean square gradient feature takes the form

$$\Phi_{g^2, \mu} = J_{g^2}^T \Sigma_\mu^{-1} J_{g^2} + J_\mu^T \Sigma_\mu^{-1} J_\mu. \quad (45)$$

The corresponding CRLB of the joint features can be obtained by

$$\text{CRLB}_{g^2, \mu} = \Phi_{g^2, \mu}^{-1}, \quad (46)$$

In (45), the FIM of the mean RSS feature can be expressed as

$$\Phi_\mu = J_\mu^T \Sigma_\mu^{-1} J_\mu, \quad (47)$$

And the FIM of mean square gradient feature in (45) can be expressed as

$$\Phi_{g^2} = J_{g^2}^T \Sigma_{g^2}^{-1} J_{g^2}, \quad (48)$$

Based on the inequality transformation method to obtain the lowest CRLB,  $\text{CRLB}_{g^2, \mu}$  can be obtained as follows:

$$\text{tr}(\text{CRLB}_{g^2, \mu}) \geq \frac{4}{\Phi_{\mu, 11} + \Phi_{\mu, 22} + \Phi_{g^2, 11} + \Phi_{g^2, 22}}, \quad (49)$$

Based on only the mean square gradient feature, the CRLB of the segment positioning takes the form

$$\text{tr}(\text{CRLB}_{g^2}) \geq \frac{4}{\Phi_{g^2, 11} + \Phi_{g^2, 22}}, \quad (50)$$

Since  $\Phi_{\mu, 11} + \Phi_{\mu, 22} + \Phi_{g^2, 11} + \Phi_{g^2, 22} > \Phi_{g^2, 11} + \Phi_{g^2, 22}$ , thus  $\text{tr}(\text{CRLB}_{g^2, \mu}) < \text{tr}(\text{CRLB}_{g^2})$ . The proof of Proposition 2 is completed.

#### APPENDIX D: PROOF OF PROPOSITION 3

Suppose the  $K$ th BS's signals of the  $l$ th segment change within a specified threshold, thus the distances of positions in this segment equivalently satisfy  $d_{1,K}^l \approx d_{2,K}^l \cdots \approx d_{N_l,K}^l$ . By plugging (32) and (33) into (48), the trace element of the  $\Phi_{g^2}$  can be expressed as follows:

$$\Phi_{g^2, 11} = \frac{16 \cdot 10^4}{(N_l - 1)^2 \ln^2 10} \sum_{k=1}^K \frac{\beta_k^l}{\rho_k^l} \left[ \sum_{i=1}^{N_l-1} (\log d_{i+1,k}^l - \log d_{i,k}^l) \left( \frac{\cos \theta_{i+1,k}^l (i+1)}{d_{i+1,k}^l} - \frac{\cos \theta_{i,k}^l i}{d_{i,k}^l} \right) \right]^2, \quad (51)$$

$$\Phi_{g^2, 22} = \frac{16 \cdot 10^4}{(N_l - 1)^2 \ln^2 10} \sum_{k=1}^K \frac{\beta_k^l}{\rho_k^l} \left[ \sum_{i=1}^{N_l-1} (\log d_{i+1,k}^l - \log d_{i,k}^l) \left( \frac{\sin \theta_{i+1,k}^l (i+1)}{d_{i+1,k}^l} - \frac{\sin \theta_{i,k}^l i}{d_{i,k}^l} \right) \right]^2. \quad (52)$$

Since the  $d_{1,K}^l \approx d_{2,K}^l \cdots \approx d_{N_l,K}^l$ , thus  $\sum_{i=1}^{N_l-1} (\log d_{i+1,K}^l - \log d_{i,K}^l) = 0$ . By plugging (51) and (52) into (50), due to  $\sum_{i=1}^{N_l-1} (\log d_{i+1,K}^l - \log d_{i,K}^l) = 0$ , thus the  $\text{CRLB}_K = \text{CRLB}_{K-1}$ . The proof of Proposition 3 is completed.

#### REFERENCES

- [1] Y. Yu, R. Chen, W. Shi, and L. Chen, "Precise 3D indoor localization and trajectory optimization based on sparse Wi-Fi FTM anchors and built-in sensors," *IEEE Trans. Veh. Technol.*, vol. 71, no. 4, pp. 4042–4056, Apr. 2022.
- [2] EUSPA, "The earth observation (EO) and global navigation satellite system (GNSS) market report," [Online], Jan. 2022, <https://space-economy.esa.int/article/126/euspa-publishes-eo-and-gnss-market-report-2022>.
- [3] Q. D. Vo and P. De, "A survey of fingerprint-based outdoor localization," *IEEE Commun. Surv. Tutor.*, vol. 18, no. 1, pp. 491–506, 1Q. 2016.
- [4] K. Jian, N. Xiaoji, and C. Xingeng, "Robust pedestrian dead reckoning based on MEMS IMU for smartphones," *IEEE Sens. J.*, vol. 18, no. 5, p. 1391–1409, May 2018.
- [5] J. A. del Peral-Rosado, R. Raulefs, J. A. López-Salcedo, and G. Seco-Granados, "Survey of cellular mobile radio localization methods: From 1G to 5G," *IEEE Commun. Surv. Tutor.*, vol. 20, no. 2, pp. 1124–1148, Secondquarter 2018.
- [6] Y. Zakaria and L. Ivanek, "Performance evaluation of UE location techniques in LTE networks," *Am. J. Sci.*, vol. 14, no. 1, pp. 81–89, Jan. 2017.
- [7] D. Floarea and V. Sgârciu, "Indoor positioning using cell of origin and LANDMARC approach," in *Proc. 2020 12th Int. Conf. Electronics, Comput. Artif. Intell. (ECAI)*, Bucharest, Romania, Jun. 2020, pp. 1–5.
- [8] D. Li, X. Chu, L. Wang, Z. Lu, S. Zhou, and X. Wen, "Performance evaluation of E-CID based positioning on OAI 5G-NR testbed," in *Proc. 2022 IEEE/CIC Int. Conf. Commun. China (ICCC)*, Sanshui, Foshan, China, Aug. 2022, pp. 832–837.
- [9] M. Borenovic, M. Simic, A. Neskovic, and M. Petrovic, "Enhanced Cell-ID + TA GSM positioning technique," in *Proc. EUROCON 2005 - Int. Conf. "Computer as a Tool"*, vol. 2, Belgrade, Serbia, Nov. 2005, pp. 1176–1179.
- [10] C. Laoudias, A. Moreira, S. Kim, S. Lee, L. Wirola, and C. Fischione, "A survey of enabling technologies for network localization, tracking, and navigation," *IEEE Commun. Surv. Tutor.*, vol. 20, no. 4, pp. 3607–3644, Fourthquarter 2018.
- [11] Z. Xiao and Y. Zeng, "An overview on integrated localization and communication towards 6G," *Sci. China Inf. Sci.*, vol. 65, no. 3, pp. 1869–1919, Dec. 2021.
- [12] K. Meng, Q. Wu, S. Ma, W. Chen, K. Wang, and J. Li, "Throughput maximization for UAV-enabled integrated periodic sensing and communication," *IEEE Trans. Wireless Commun.*, vol. 22, no. 1, pp. 671–687, Jan. 2023.
- [13] A. Abolfathi Momtaz, F. Behnia, R. Amiri, and F. Marvasti, "NLOS identification in range-based source localization: Statistical approach," *IEEE Sens. J.*, vol. 18, no. 9, pp. 3745–3751, May 2018.
- [14] C. Gentner, M. Ulmschneider, I. Kuehner, and A. Dammann, "WiFi-RTT indoor positioning," in *Proc. 2020 IEEE/ION Position, Locat. Navig. Symp. (PLANS)*, Portland, OR, USA, Apr. 2020, pp. 1029–1035.
- [15] C. Huang, A. F. Molisch, R. Wang, P. Tang, R. He, and Z. Zhong, "Angular information-based NLOS/LOS identification for vehicle to vehicle MIMO system," in *Proc. 2019 IEEE Int. Conf. Commun. workshops (ICC Workshops)*, Shanghai, China, May 2019, pp. 1–6.
- [16] F. Carpi, L. Davoli, M. Martalò, A. Cilfone, Y. Yu, Y. Wang, and G. Ferrari, "RSSI-based methods for LOS/NLOS channel identification in indoor scenarios," in *Proc. 2019 16th Int. Symp. Wirel. Commun. Syst. (ISWCS)*, Oulu, Finland, Aug. 2019, pp. 171–175.
- [17] F. Xiao, Z. Guo, H. Zhu, X. Xie, and R. Wang, "AmpN: Real-time LOS/NLOS identification with WiFi," in *Proc. 2017 IEEE Int. Conf. Commun. (ICC)*, Paris, France, May 2017, pp. 1–7.
- [18] T. Van Nguyen, Y. Jeong, H. Shin, and M. Z. Win, "Machine learning for wideband localization," *IEEE Journal on Selected Areas in Communications*, vol. 33, no. 7, pp. 1357–1380, Jul. 2015.
- [19] S. Maranò, W. M. Gifford, H. Wymeersch, and M. Z. Win, "NLOS identification and mitigation for localization based on UWB experimental data," *IEEE Journal on Selected Areas in Communications*, vol. 28, no. 7, pp. 1026–1035, Sep. 2010.

- [20] Y. Zhang, J. Ren, and W. Chen, "A ToA-based location algorithm reducing the NLOS error under location-aware networks," in *Proc. 2011 7th Int. Conf. Wirel. Commun., Networking and Mob. Computing*, Wuhan, China, Sep. 2011, pp. 1–4.
- [21] Y. Chan and K. Ho, "A simple and efficient estimator for hyperbolic location," *IEEE Trans. Signal Process.*, vol. 42, no. 8, pp. 1905–1915, Aug. 1994.
- [22] X. Cai, X. Li, R. Yuan, and Y. Hei, "Identification and mitigation of NLOS based on channel state information for indoor WiFi localization," in *Proc. 2015 Int. Conf. Wirel. Commun. Signal Process. (WCSP)*, Nanjing, China, Dec. 2015, pp. 1–5.
- [23] G. Pecoraro, E. Cianca, S. Di Domenico, and M. De Sanctis, "LTE signal fingerprinting device-free passive localization robust to environment changes," in *Proc. Glob. Wireless Summit (GWS)*, Chiang Rai, Thailand, Nov. 2018, pp. 114–118.
- [24] D. Xiaochao, S. Xiong, H. Zhanjun, H. Yaning, and H. Yili, "Indoor localization method based on CSI in complex environment," *Chinese J. Internet Things (CJIOT)*, vol. 2, no. 4, pp. 68–77, Nov. 2018.
- [25] M. Yang, D. R. Jackson, J. Chen, Z. Xiong, and J. T. Williams, "A TDOA localization method for nonline-of-sight scenarios," *IEEE Trans. Antennas Propag.*, vol. 67, no. 4, pp. 2666–2676, Apr. 2019.
- [26] W. Fuzhan, Z. Xiaorong, C. Meijuan, and Z. Hongbo, "High-precision indoor wireless positioning method based on generative adversarial network," *Chinese J. Internet Things (CJIOT)*, vol. 5, no. 2, pp. 107–115, Jun. 2021.
- [27] X. Tian, X. Wu, H. Li, and X. Wang, "RF fingerprints prediction for cellular network positioning: A subspace identification approach," *IEEE Trans. Mob. Comput.*, vol. 19, no. 2, pp. 450–465, Feb. 2020.
- [28] S. G. Lee and C. Lee, "Developing an improved fingerprint positioning radio map using the K-Means clustering algorithm," in *Proc. 2020 Int. Conf. Information Networking (ICOIN)*, Barcelona, Spain, Jan. 2020, pp. 761–765.
- [29] Y. Mo, Z. Cao, and B. Wang, "Occurrence-based fingerprint clustering for fast pattern-matching location determination," *IEEE Commun. Lett.*, vol. 16, no. 12, pp. 2012–2015, 2012.
- [30] B. Huang, R. Yang, B. Jia, W. Li, and G. Mao, "A theoretical analysis on sampling size in WiFi fingerprint-based localization," *IEEE Trans. Veh. Technol.*, vol. 70, no. 4, pp. 3599–3608, Apr. 2021.
- [31] P.-H. Tseng and K.-T. Lee, "A femto-aided location tracking algorithm in LTE-A heterogeneous networks," *IEEE Trans. Veh. Technol.*, vol. 66, no. 1, pp. 748–762, 2017.
- [32] M. Mahbub and B. Barua, "Optimal positioning of macro base station: An approach to ensure optimal coverage of small cell in HetNet," in *Proc. Conf. Electron. Comput. Commun. Technol. (CONECT)*, Bangalore, India, Dec. 2021, pp. 1–4.
- [33] K. Meng, Q. Wu, W. Chen, and D. Li, "Sensing-assisted communication in vehicular networks with intelligent surface," *IEEE Trans. Veh. Technol.*, vol. 73, no. 1, pp. 876–893, Jan. 2024.
- [34] J. Hao, Z. Hongming, and T. Liu, *Novel Sum-of-Sinusoids Simulation Channel Modeling for 6G Multiple-Input Multiple-Output Vehicle-to-Everything Communications*, vol. 21, no. 1, pp. 242–259, Jan. 2024.
- [35] D.-N. Vu, N.-N. Dao, D. Won, and S. Cho, "Potential enabling technologies for 6g mobile communication networks: A recent review," in *Proc. 2023 Fourteenth Int. Conf. Ubiquitous Future Netw. (ICUFN)*, Paris, France, Jul. 2023, pp. 631–635.
- [36] D. Yan, K. Guan, D. He, J. Kim, H. Chung, D. Tian, and Z. Zhong, "Blockage effects of road bridge on mmWave channels for intelligent autonomous vehicles," *IEEE Trans. Intell. Transp. Syst.*, vol. 25, no. 3, pp. 2908–2919, Mar. 2024.
- [37] P. Chen, J. Shang, and F. Gu, "Learning RSSI feature via ranking model for Wi-Fi fingerprinting localization," *IEEE Trans. Veh. Technol.*, vol. 69, no. 2, pp. 1695–1705, Feb. 2020.
- [38] J. Wang, J. Luo, S. J. Pan, and A. Sun, "Learning-based outdoor localization exploiting crowd-labeled WiFi hotspots," *IEEE Trans. Mob. Comput.*, vol. 18, no. 4, pp. 896–909, Apr. 2019.
- [39] S. Xu, "Optimal sensor placement for target localization using hybrid RSS, AOA and TOA measurements," *IEEE Communications Letters*, vol. 24, no. 9, pp. 1966–1970, Sep. 2020.
- [40] G. Chandrasekaran, T. Vu, A. Varshavsky, M. Gruteser, R. P. Martin, J. Yang, and Y. Chen, "Tracking vehicular speed variations by warping mobile phone signal strengths," in *Proc. IEEE Pervasive Comput. Commun. (PerCom)*, Seattle, WA, USA, Mar. 2011, pp. 213–221.
- [41] C. Truong, L. Oudre, and N. Vayatis, "Selective review of offline change point detection methods," *Signal Processing*, vol. 167, no. 1, pp. 107–299, 2020.
- [42] B. Wang, S. Zhou, W. Liu, and Y. Mo, "Indoor localization based on curve fitting and location search using received signal strength," *IEEE Trans. Ind. Electron.*, vol. 62, no. 1, pp. 572–582, Jan. 2015.
- [43] P. Newson and J. Krumm, "Hidden markov map matching through noise and sparseness," in *Proc. ACM SIGSPATIAL Int. Conf. Adv. Geogr. Inf. Syst.*, Seattle, WA, USA, Nov. 2009, pp. 336–343.
- [44] R. V. Akhpashev and A. V. Andreev, "COST 231 Hata adaptation model for urban conditions in LTE networks," in *Proc. 2016 17th Inter. Conf. Young Spec. Micro/Nanotechnologies Elec. Dev. (EDM)*, Erlagol, Russia, Jul. 2016, pp. 64–66.
- [45] T. Report, "—TR 138 901 - V14.0.0 - 5G; Study on channel model for frequencies from 0.5 to 100 GHz (3GPP TR 38.901 version 14.0.0 Release 14)," 2017.
- [46] G. Chen, X. Guo, K. Liu, X. Li, and J. Yang, "RWKNN: A modified WKNN algorithm specific for the indoor localization problem," *IEEE Sensors Journal*, vol. 22, no. 7, pp. 7258–7266, Apr. 2022.
- [47] S. Liu, R. de Lacerda, and J. Fiorina, "Hierarchical fingerprinting and feature extraction for indoor localization," in *2022 IEEE Inter. Conf. Commun. (ICC)*, Seoul, Korea, May 2022, pp. 4637–4642.
- [48] Y. Shu, Y. Huang, J. Zhang *et al.*, "Gradient-based fingerprinting for indoor localization and tracking," *IEEE Trans. Ind. Electron.*, vol. 63, no. 4, pp. 2424–2433, Apr. 2016.
- [49] "Recommendation ITU-R P.1411-11 - propagation data and prediction methods for the planning of short-range outdoor radiocommunication systems and radio local area networks in the frequency range 300 MHz to 100 GHz." Geneva: Electronic Publication, Sep. 2021.
- [50] D. Li, Y. Lei, and H. Zhang, "A novel outdoor positioning technique using LTE network fingerprints," *Sensors*, vol. 20, no. 6, pp. 1691–1710, Mar. 2020.
- [51] R. Alieiev, T. Hehn, A. Kwoczek, and T. Kürner, "Predictive communication and its application to vehicular environments: Doppler-shift compensation," *IEEE Trans. Veh. Technol.*, vol. 67, no. 8, pp. 7380–7393, Aug. 2018.
- [52] L. Cong, "Multi-scale vehicle localization algorithm," [Online], Jul. 2024, <https://v.qq.com/x/page/u3558vfp0y6.html>.
- [53] B.-J. Chang, W. Hung, Y. Lin, and W.-T. Chang, "Dynamic keeping reserved resource probability with slicing flow steering in 5G sidelink SPS for platooning ADAS and autonomous self driving," in *Proc. Int. Autom. Control Conf. (CACs)*, Hsinchu, Taiwan, Dec. 2020, pp. 1–6.